

NASA Technical Memorandum 89035

Noise Propagation  
From a Four-Engine,  
Propeller-Driven  
Airplane

William L. Willshire, Jr.

FEBRUARY 1987



NASA Technical Memorandum 89035

Noise Propagation  
From a Four-Engine,  
Propeller-Driven  
Airplane

William L. Willshire, Jr.  
*Langley Research Center*  
*Hampton, Virginia*

**NASA**

National Aeronautics  
and Space Administration

Scientific and Technical  
Information Branch

1987

## Contents

Summary . . . . .	1
Introduction . . . . .	1
Experiment Description . . . . .	1
General . . . . .	1
Test Airplane . . . . .	2
Data Reduction . . . . .	2
General Data Analysis Procedures . . . . .	3
Definitions . . . . .	3
Calculations . . . . .	4
Results and Discussion . . . . .	4
Lateral Attenuation . . . . .	4
Ground Effects . . . . .	6
Source Variability . . . . .	6
Source Symmetry . . . . .	7
Review of Results . . . . .	7
References . . . . .	8
Tables . . . . .	10
Figures . . . . .	11
Appendix—Results of One-Third-Octave-Band Noise Source Symmetry . . . . .	31

**PRECEDING PAGE BLANK NOT FILMED**

## Summary

A flight experiment was conducted to investigate the propagation of periodic low-frequency noise from a propeller-driven airplane. The test airplane was a large four-engine, propeller-driven airplane flown at altitudes from 15 to 500 m over the end of an 1800-m-long, 22-element microphone array. The acoustic data were reduced by a one-third-octave-band analysis. The primary propagation quantities computed were lateral attenuation and ground effects, both of which become significant at shallow elevation angles. Scatter in the measured results largely obscured the physics of the low-frequency noise propagation. Variability of the noise source, up to 9.5 dB over a 2-sec interval, was the major contributor to the data scatter. The microphones mounted at ground level produced more consistent results with less scatter than those mounted 1.2 m above ground. The generally accepted method of computing lateral attenuation utilizing overhead and sideline microphones led to misleading results with the highly directional propeller noise source. The ground noise levels were found to be greater on the port side than on the starboard side. This difference was attributed to fuselage shielding resulting from the test airplane propellers being rotated in a counterclockwise direction when viewed from the front.

## Introduction

Airplane noise propagation research to a large extent has been driven by community noise regulation issues. The propagation research has been focused on understanding and predicting the propagation of the noise of jet-powered commercial airplanes. Of particular interest has been the propagation of airplane noise at grazing angles to the ground. The interaction of the sound with the ground produces an additional attenuation of the sound. This attenuation is referred to as "ground effects" and is usually positive (a reduction) for grazing angles. Ground effects and shielding effects comprise lateral attenuation. The influence of lateral attenuation on predicted airplane noise levels and the subsequent impact on the size of noise contours led to the need for an accurate prediction of lateral attenuation. Through the auspices of the Society of Automotive Engineers (SAE) A-21 Committee on Aircraft Noise, the available lateral attenuation data for jet-powered airplanes were collected and an empirical prediction methodology for lateral attenuation was established from the ensuing data base (refs. 1 and 2).

Interest in the propagation of periodic low-frequency sound has increased with the development

of the advanced turboprop (ATP) technology. The question has been raised on the suitability of using a data base acquired from jet-powered airplanes to address issues of grazing angle propagation of propeller and helicopter noise. In an attempt to address the issue of propagation of periodic low-frequency airplane noise, a flight experiment was planned and conducted that utilized a large four-engine, turboprop-powered airplane. The primary objective of the experiment was to measure the effects of propagation of periodic low-frequency noise at grazing angles to the ground. A secondary objective of the experiment was to investigate noise source directivity and installation effects on airplane deck angle. The purpose of this report is to present the results of this flight experiment.

## Experiment Description

### General

In the fall of 1982 a flight experiment was conducted at the NASA Wallops Flight Facility to investigate the propagation of periodic low-frequency noise over grass-covered ground. The experiment had two major objectives. The first objective was to measure the propagation of low-frequency noise at grazing angles to the ground. This objective was achieved by flying a test airplane at constant speed at altitudes ranging from 15 to 500 m over the end of an 1800-m-long, 22-element microphone array positioned over grass. A second objective of the experiment was to investigate noise source directivity and installation effects on airplane deck angle. The second objective was accomplished by flying the same test airplane over the middle of the microphone array at constant speed at an altitude of 100 m at one of three different flap settings to vary the test airplane deck angle.

The flight path over the end of the microphone array was referred to as "path A." The flight path over the middle of the microphone array was referred to as "path B." Both flight paths and the microphone array are illustrated in figure 1. Note that the angle between the flight path and the microphone array for path A is approximately  $60^\circ$ . In order to fly the low-altitude path A runs safely, the test airplane was constrained to fly over a runway. The ground track of flight path A was the centerline of runway 10/28. (See fig. 1.) This flight path permitted flying the 15-m-altitude passes, thus avoiding tall obstacles like buildings and trees. For flight path B, the flight path was perpendicular to the middle of the microphone array. The altitude of path B was chosen as the lowest safe altitude for flying over Wallops for this experiment. The nominal airplane headings were

100° magnetic for flight path A and 130° magnetic for flight path B.

The 22-element microphone array consisted of 12 flush-mounted microphones and 10 microphones mounted 1.2 m above the ground. The microphones were positioned over grass, which was similar to what has been called institutional grass. An indirect method was used in an earlier propagation experiment performed at Wallops to measure the acoustic impedance of the grass-covered ground (ref. 3). A ground flow-resistance value of  $150 \text{ Mg}/(\text{sec}\cdot\text{m}^3)$  was found to represent the impedance of the grass-covered surface in a locally reacting model of impedance.

Weather information was obtained for the testing periods using a balloon system that made profiles up to the highest airplane altitude. An 18-transducer weather instrument was used to profile from ground level up to 6 m.

### Test Airplane

The test airplane for the experiment was a Lockheed 188 Electra. Figures 2 and 3 show a photograph and a three-view drawing, respectively, of the test airplane. The empty weight of the airplane was approximately 26 000 kg and it was powered by four 4050-eshp (equivalent shaft horsepower) turboprop engines. To fly the constant low-speed runs for the propagation experiment, the four engines were operated at power settings from 850 to 1000 eshp. Each engine turned a four-blade 4.1-m-diameter propeller. The propellers were manufactured by Aeroproducts and had a model number of A6441FN-606. The propellers turned counterclockwise when viewed from the front. The engines ran at 13 820 rpm and the propellers turned at a constant 1020 rpm. The blade-tip rotational speed was 215 m/sec and the fundamental blade passage frequency was 68 Hz. The test airplane was instrumented with a microphone mounted on the starboard wingtip boom in the plane of the closest propeller, roughly 1.5 propeller diameters away. The test airplane flew all the data runs with the landing gear retracted. The test airplane was equipped with a laser reflector that may be seen in figure 2 and was tracked with a laser/radar tracker during the experiment. The nominal airplane speed for both flight paths was 70 m/sec.

The completed test matrix for the experiment is given in table I. Forty-one flight path A runs were made at altitudes varying from 15 to 500 m. All flight path A runs except one were made with a 78-percent flap setting. Sixteen flight path B runs were made at an altitude of 100 m. For flight path B, three flap settings of 0, 78, and 100 percent were used. The airplane deck angles associated with the three flap

angles flown were 8°, 5°, and 2°, respectively, in the nose-up direction.

### Data Reduction

The acoustic data have been reduced to one-third-octave-band time histories using standard procedures. The result of this reduction is a succession of  $\frac{1}{4}$ -sec averaged one-third-octave-band spectra. The frequency range of each spectrum is from 20 Hz to 25 kHz. In the data analysis process, to be explained in more detail in the next section, two  $\frac{1}{4}$ -sec one-third-octave-band spectra are averaged to form an effective  $\frac{1}{2}$ -sec averaged result. Data were rejected from runs in which the ground tracks of the test airplane were more than 25 m from the desired ground track. To be considered valid, the measured acoustic data had to have a 3-dB or greater signal-to-noise ratio. The noise levels used were the measured ambient levels at the beginning of a run when the test airplane was more than 1800 m away from the microphone array.

Both the tracking data and the weather balloon profile data have been reduced and organized into a computer data base along with the acoustic data. The tracking data are illustrated for flight paths A and B in figures 4 and 5, respectively. The data reduction coordinate system and microphone (mic) numbering method are also illustrated in these figures.

The data reduction coordinate system is a right-hand Cartesian system with the origin at microphone 19. The X-axis is the centerline of the runway beside which the microphones were deployed. (See runway 04/22, in fig. 1.) The flight direction is from positive Y to negative Y. The even-numbered microphones are 1.2-m microphones (mounted 1.2 m above ground); the odd-numbered microphones are flush-mounted (ground level) microphones. The coordinates of the microphones are given in table II. The third column in table II is the actual Z-coordinate of each microphone with respect to the origin, microphone 19, when taking topography into account.

An example of weather balloon data is given in figure 6. Temperature, wind speed, wind direction, and relative humidity profiles are given in figures 6(a) through 6(d), respectively. The weather data in figure 6 were measured on October 3, 1982, and are typical of the period in which acoustic data were taken on this day. Later, in the section entitled "Results and Discussion," the acoustic data taken on this day will be emphasized. On this day the temperature gradient was lapse, the wind speed was low (less than 2 m/sec), the wind direction was roughly in the direction of the test airplane flight paths, and the

relative humidity was less than 80 percent. A temperature lapse is defined as temperature decreasing with height and is the normal condition in the afternoon of a sunny day.

## General Data Analysis Procedures

### Definitions

The results to be presented will include lateral attenuation and ground effects plotted against slant range and elevation angle. Definitions of slant range and elevation angle, as well as of lateral attenuation and ground effects, are illustrated in figure 7. The slant range  $R$  is the distance from the microphone to the noise source at a defined position. The elevation angle is the angle between a horizontal line and the line connecting the microphone and noise source. Lateral attenuation is defined as the difference in sound pressure level between overhead and sideline measurements at the sideline slant range. With this definition, the effects of spherical spreading and atmospheric absorption are ideally the same for both paths and, therefore, do not affect the lateral attenuation results. Directivity differences (including source shielding), ground absorption, and ground reflection are included in lateral attenuation.

Obtaining overhead and sideline measurements at the same slant range is normally accomplished in one of two ways. For each measurement of lateral attenuation, two airplane passes can be required. One airplane flyby is used to make a measurement at a sideline microphone for a certain slant range. A second airplane flyby at a higher altitude is used to make an overhead measurement at the same slant range. This technique requires more airplane passes and the weather or the airplane setup state may vary between the two passes needed for a single measurement of lateral attenuation. Another method used to measure lateral attenuation requires a single pass over a microphone array. In this technique a sideline microphone is used to make a sideline measurement that defines a slant range. For the same pass an overhead microphone is used to make an overhead measurement, which is for a smaller slant range than the sideline measurement. The overhead measurement is corrected to the sideline slant range mathematically by using corrections for spherical spreading and atmospheric absorption. The atmospheric absorption corrections are either calculated using standard procedures with measured weather data as input or empirically derived from measured overhead data for different altitude passes.

Ground effects are defined as the difference between a sideline sound pressure level and a free field

sound pressure level for the same propagation distance. Ideally in a ground effects result, the effects of spherical spreading, atmospheric absorption, and source directivity are removed and the result is a measure of the interaction between the airplane noise and the reflecting surface. In ground effects measurements, a flush-mounted overhead microphone is normally used to estimate the free field level, which is defined as being 6 dB less than the overhead measured results obtained from using a flush-mounted microphone (ref. 4). For meaningful results using this technique to define the free field level, the source must exhibit source directivity symmetry. That is, the directivity of the source must be the same for the overhead and sideline measurements.

In both ground effects and lateral attenuation measurements, the influence of refraction, diffraction, turbulent scattering, and other propagation anomalies are inherent in the measurements and to some degree affect the computed results. The experimental design should minimize the effects of these phenomena. If uncontrolled, the effects of these propagation anomalies can dominate the trends observed in the data. Unless careful and extensive weather measurements are made, it is difficult to separate the different effects and to reach general conclusions that are applicable to anything except the data base from which they were obtained. To minimize the effects of these propagation anomalies in the present experiment, the weather conditions acceptable for taking data were such as to minimize the effects of refraction and turbulent scattering. This minimization was done by testing on days with low wind and with temperature gradients close to 0.

Lateral attenuation and ground effects may be computed in any number of noise metrics. Lateral attenuation is usually computed in frequency-integrated metrics like overall sound pressure level (OASPL) and A-weighted sound pressure level (LA) or in frequency and time-integrated metrics like sound exposure level (SEL) and effective perceived noise level (EPNL). Ground effects are usually computed as sound pressure level (SPL) as a function of frequency, either one-third-octave band or narrow band.

Lateral attenuation and ground effects may be computed with either 1.2-m or ground-mounted microphones, although lateral attenuation is traditionally computed with 1.2-m microphones. When lateral attenuation is computed with 1.2-m microphones, both the sideline and overhead microphones are 1.2-m microphones. As a consequence, the result contains the difference of two different interference patterns caused by the interaction of the direct and reflected signals received by microphones positioned

above the ground. Ground effects results contain the influence of only one interference pattern, the one due to the sideline microphone if it is mounted above the ground. An additional observation about lateral attenuation and ground effects is that there is a sign difference between them. Ground absorption produces a positive value of lateral attenuation and a negative value of ground effects.

### Calculations

Lateral attenuation results for the present paper were calculated with the following procedures. For this study, lateral attenuation is computed using microphones positioned 1.2 m above the ground, denoted by the even-numbered microphones in this experiment. To compute lateral attenuation for a particular sideline microphone and run, the position of the test airplane is found in which the sound emitted at this position propagates parallel and above the microphone array to the particular microphone. When comparing lateral attenuation results from different microphones in the microphone array, it is important that the acoustic data used in the lateral attenuation computations have the same source azimuthal emission angle and that the acoustic data have propagated over the same ground. Constraining the source azimuthal emission angle minimizes the consequence of Doppler frequency shift in the computed results.

The airplane position in which the sound emitted propagates over the microphone array is called the overhead position in this paper. The overhead position is found for both the sideline and overhead microphones. To find the overhead positions in this experiment, the airplane positions were found that have the same *Y*-coordinate as the sideline and overhead microphones. Recall that the *Y*-axis of the data reduction coordinate system is perpendicular to the microphone array. The position of the test airplane having the same *Y*-coordinate as a microphone is the position of the airplane at which the sound emitted propagates parallel and above the microphone array to the particular microphone. The overhead position of the sideline microphone defines the values of slant range and elevation angle associated with a value of lateral attenuation.

The reception times are computed for the sideline and overhead microphones for the sound emitted at the overhead positions. Average values of the sound speed are calculated from the measured weather profiles and are used in the reception time calculations. The two  $\frac{1}{4}$ -sec averaged one-third-octave-band spectra received at each microphone closest to the computed reception times are averaged. The overhead-microphone averaged spectrum is propagated to the

slant range of the sideline-microphone averaged spectrum by using spherical spreading and atmospheric absorption corrections. The atmospheric absorption corrections are computed according to the standard method of the American National Standards Institute (ANSI) using averaged measured weather profile data. (See ref. 5.) For OASPL lateral attenuation results, the sideline averaged spectrum and the slant-range-corrected, overhead averaged spectrum are integrated to form the OASPL metric. The sideline value is then subtracted from the overhead value.

To calculate a ground effects result, microphone 19, a flush-mounted microphone, is used for the overhead microphone. A  $\frac{1}{2}$ -sec averaged spectrum is computed as in the calculation procedures for lateral attenuation. An estimate of the free field level is formed by subtracting 6 dB from the overhead averaged spectrum. Subtracting 6 dB is done to account for pressure doubling of a flush-mounted microphone (ref. 4). The free field spectrum is then propagated to the sideline-microphone slant range, as described in the preceding section, to form a slant-range-corrected, free field spectrum, which is then subtracted from the measured sideline spectrum to form a one-third-octave-band ground effects spectrum. For both lateral attenuation and ground effects calculations, the sideline and overhead spectra are generated for each run.

## Results and Discussion

### Lateral Attenuation

Lateral attenuation results are given in figure 8 for all the flight path A data for the 1.2-m microphones. In figure 8 the data are presented to illustrate the nominal test airplane altitude associated with each data point. The lateral attenuation results presented in figure 8 are in the OASPL metric and are plotted against elevation angle. The zero values of lateral attenuation for large elevation angles are caused by the data analysis software when the sideline and overhead microphones are the same. By definition, lateral attenuation is 0 underneath the flight path when the sideline and overhead microphones become the same microphone. The data exhibit excessive scatter. The 90-percent chi-square confidence limits for a single data point, based on the bandwidth of the 63-Hz one-third-octave band and the effective  $\frac{1}{2}$ -sec averaged time, are  $-2.9$  to  $4.7$  dB. These limits are worst-case numbers based on a random data assumption. The noise signal of the Lockheed 188 is periodic with major contributions from the blade passage frequency (BPF) harmonics. The second-order least-squares fit to the data in figure 8, denoted by the solid curve, is a means of averaging the

collective data set. However, it is difficult to reach meaningful conclusions with data having as much scatter as that seen in figure 8.

The data in figure 8 are replotted in figure 9 with the elimination of the 15-m-altitude runs, since these runs may introduce erroneous results because of the low altitude. Directivity smearing is an averaging over the directivity angle and possible noise sources caused by the range of directivity angles covered by a particular averaging time, which is a function of airplane position, speed, and altitude. Directivity smearing increases in general with increased speed and decreased altitude. The lateral attenuation results of figure 9 still exhibit excessive scatter. The least-squares-fit curve tends toward larger values of lateral attenuation for smaller elevation angles, an indication that the 15-m-altitude runs were associated with smaller values of lateral attenuation than the higher altitude runs.

The scatter observed in the results given in figures 8 and 9 is due in part to the measurement uncertainty mentioned earlier, but the quantity of data scatter observed is not totally explained by measurement uncertainty. Other factors have contributed to the scatter. The weather during the test was good to fair. Prevailing winds were parallel to the flight path and tended to reduce refraction due to wind gradients in the direction of propagation from the overhead test airplane position to the microphone array. In general, the data were measured under slight temperature-lapse gradients, a condition which would tend to increase the values of lateral attenuation due to the upward refraction. Interference effects between the four propellers may have possibly contributed to the data scatter. Propeller source variability and microphone height effects may also have been factors.

In figure 10(a) lateral attenuation results in OASPL are plotted versus elevation angle for ground-mounted microphones for selected runs on path A. The data points are plotted in order to identify the microphones associated with each data point. The data used to calculate the results given in figure 10(a) were taken on October 3, 1982. The nominal weather for this day was illustrated in figure 6 and was judged to be very good for an outdoor acoustic test. A 6-dB signal-to-noise level criterion was used in the lateral attenuation calculations. The selection criteria, day and signal-to-noise level, have reduced the number of data points in figure 10 over those in the previous result figures. The scatter in the results has been reduced and a trend of increasing lateral attenuation with decreasing elevation angle is seen.

In figure 10(b) lateral attenuation results are given for the same data runs as in figure 10(a) but

for the 1.2-m-microphones. The 1.2-m-microphone results exhibit increased data scatter with generally lower and, in fact, negative values of lateral attenuation than those for the ground-mounted microphones. Negative values of lateral attenuation indicate that the sideline measured value is greater than the overhead measured value at the sideline propagation distance. The increased scatter of the 1.2-m-microphone results is caused by the interference patterns associated with microphones positioned above the ground. The difference operation taken between two spectra in computing lateral attenuation accentuates the differences in the two interference patterns causing the data scatter to increase.

The consequence of the directivity angle associated with the overhead position for flight path A, which is  $122.5^\circ$  referenced to the forward direction, was unknown. This angle is off the expected maximum directivity of  $90^\circ$  for propeller noise. To check for an effect, lateral attenuation results were computed using flight path B runs in which the directivity angle of the overhead position is  $90^\circ$ . Lateral attenuation results in OASPL computed from flight path B runs are given in figure 11(a) for ground-mounted microphones and in figure 11(b) for 1.2-m microphones. In general, the lateral attenuation results for flight path B exhibit slightly more data scatter with more negative values than the flight path A results. The 1.2-m-microphone results for flight path B when compared with the ground-mounted results have increased scatter and a trend toward smaller and negative values of lateral attenuation.

The increased scatter of the flight path B results including negative values of lateral attenuation may be caused by interference effects between the four propellers. The maxima and minima of the multisource interference would add scatter to the measurements in the same manner that interference effects increased the data scatter. The multisource interference would, in general, be different for the sideline and overhead measurements. This difference would be accentuated by the different operation in the lateral attenuation computational process. Multisource interference would be expected to be greater for the overhead microphone, which is under the flight path, than for the sideline microphone, which is to the side of the flight path and does not have a line of sight to all four propellers. The flight path B measurements have a greater BPF harmonic content than the flight path A measurements because of the directivity angles associated with the overhead positions of the two flight paths. Multisource interference would be expected to have a more dominant effect on flight path B results than on flight path A results. It is difficult to separate the effects of

multisource and direct/reflected interference from data from microphones positioned above the ground.

Lateral attenuation results in A-weighted SPL (LA) for the data obtained on October 3, 1982, for flight path A runs are given in figure 12(a) for the ground-mounted microphones and in figure 12(b) for the 1.2-m microphones. The frequency weighting characteristics of A-weighting are such as to de-emphasize the BPF harmonics or the periodic low-frequency portion of the test airplane noise source. The ground-mounted results (fig. 12(a)) show a negative dip for elevation angles roughly between  $10^\circ$  and  $30^\circ$ . Similar negative dips of lateral attenuation for jet-powered commercial airplanes are noted in reference 2 for airplanes with wing-mounted engines. The primary reasons for the dip given in the reference are airplane configuration and engine installation effects leading to refraction of the airplane noise through wingtip or flap-edge vortices. The 1.2-m results in figure 12(b) again are shifted downward on the lateral attenuation plot. The directivity angle of the overhead position of the flight path A data ( $122.5^\circ$ ) should cause the jet exhaust noise of the four engines to make larger contributions to the measured data of the sideline and overhead positions. The A-weighting should also tend to emphasize the jet exhaust noise.

In previous studies (ref. 6), jet-powered airplanes were used successfully in lateral attenuation flight experiments performed at the Wallops Flight Facility with similar flight path and microphone layout geometries as used in the present experiment. The lateral attenuation results of these experiments were consistent and had less data scatter than the present results. The 90-percent confidence limits for these experiments were the same as in the current experiment, but lateral attenuation trends with propagation distance and elevation angle were clearly discernible in the previous experimental results. The increased data scatter observed in the present study is attributable to the nature of the acoustic sources of the test airplane.

The LA lateral attenuation results for flight path B (fig. 13) have less scatter than the corresponding results for flight path A. The ground-mounted-microphone results (fig. 13(a)) show a general trend of increasing lateral attenuation with decreasing elevation angle. The 1.2-m-microphone results (fig. 13(b)) again show the influence of microphone interference patterns due to direct/reflected paths or multisource interference lowering the values of lateral attenuation.

Lateral attenuation results are presented in figure 14 for flight path A for the one-third-octave band containing the BPF (the 63-Hz band). The results for the ground-mounted microphones are presented

in figure 13(a). The results again have considerable scatter. The BPF lateral attenuation results increase from 0 at overhead to approximately 15 dB at elevation angles less than  $20^\circ$ . At smaller elevation angles the value of lateral attenuation is roughly constant. The 1.2-m-microphone results are given in figure 14(b). The effect of the 1.2-m microphones is again to lower the value, including negative values, of lateral attenuation as compared with the ground-mounted results.

Lateral attenuation results in BPF SPL for flight path B are given in figures 15(a) and 15(b) for ground-mounted and 1.2-m microphones, respectively. Greater scatter is shown for flight path B than for flight path A, with a lowering of values for the 1.2-m results as compared with the ground-mounted-microphone results. This increase in scatter for flight path B is again explained by the increased effects of multisource interference in the flight path B results.

### Ground Effects

Ground effects calculations were performed with the BPF one-third-octave-band data taken on October 3, 1982, for ground-mounted microphones. The results are given in figure 16 as a function of elevation angle. The open symbols are the calculated ground effects from the measured data. The shaded band represents the range of corresponding ground effects predictions using the ground effects model developed in reference 7 and used in reference 6. A value of  $100 \text{ Mg}/(\text{sec}\cdot\text{m}^3)$  was used to model the acoustic impedance of the grass-covered ground that the microphones were positioned over. In reference 6 this value of ground flow resistance was found to give good agreement between measured and predicted ground effects for jet-airplane noise and is close to the indirectly measured value of  $150 \text{ Mg}/(\text{sec}\cdot\text{m}^3)$  found in reference 3. The particular geometry between the sideline microphone and the test airplane obtained from the laser tracker data was used as input to the ground effects model.

To interpret these results it is necessary to recall the sign difference between lateral attenuation and ground effects. A negative value of ground effects and a positive value of lateral attenuation indicate that the sideline measurement is less than the free field or the overhead measurement at the same slant range. The ground effects predictions in figure 16 form an upper bound on the measured values of ground effects. The measured data exhibit a lot of scatter, and large negative values occur for large elevation angles. The disagreement between theory and measurement indicates that the measured results are strongly influenced by a phenomenon not modeled.

Multisource interference and source variability may explain the observed scatter.

### Source Variability

To check the variability of the source, the BPF SPL is plotted against airplane altitude in figure 17 for an overhead ground-mounted microphone. The data are for the flight path A runs flown on October 3, 1982. The horizontal axis in figure 17 could be labeled either "slant range" or "altitude" because of the ground-mounted microphones. The measured BPF levels exhibit up to 10 dB variability for the same altitude. In spite of the scatter, the data show a spherical spreading trend, that is, a 6-dB decrease in level per doubling of distance.

Time histories of the test airplane wing-mounted boom microphone are given in figure 18. The boom was mounted on the starboard wing so that the microphone was in the plane of rotation of the closest propeller, approximately 1.5 rotor diameters away from the propeller hub. In figure 18 the root-mean-square voltage  $V_{\text{rms}}$  of the BPF is plotted against time for two runs. Figure 18(a) presents a time history for a 500-m-altitude run, and figure 18(b) presents a time history for a 15-m-altitude run. The character of the two time histories is different. The amplitude of the higher altitude time history varies smoothly for a period of approximately 10 sec. The lower altitude time history varies more rapidly with large amplitude changes occurring in small time increments of approximately 2 sec. Although the nature of the two time histories has this subjective difference, both show over a 9.5-dB variability with time. This source variability caused much of the scatter observed in the measured results. Undoubtedly, multisource interference, microphone height, directivity, and measurement uncertainty effects have also contributed to the observed data scatter, but the source itself appears to be the major contributor.

### Source Symmetry

The flight path B data taken on October 6, 1982, have been integrated to form the sound exposure level (SEL) metric. For the ground microphones for flight path B, the SEL results are plotted as a function of the slant range of the closest approach point in figure 19 to illustrate the port/starboard symmetry of the test airplane noise. The sketch of the test airplane in the middle of the figure illustrates that the four propellers rotated in a counterclockwise direction when viewed from the front. The SEL values on the port side of the airplane are larger than those on the starboard side. The rate of decay of noise level with slant range is less on the port side than on the starboard side. The microphone 19 data (denoted

by the open square symbols) appear to be high with respect to the rest of the data. However, eliminating the microphone 19 data does not alter the conclusion that the port-side SEL levels are greater than the starboard-side levels. Fuselage shielding of the radiated propeller noise may explain this asymmetry. The port-side propellers turn toward the fuselage from the top of the propeller disk. The starboard propellers turn toward the fuselage from the bottom of the propeller disk. Thickness noise (the dominant BPF noise source in the propeller plane for the test airplane) radiates tangentially from the blade tips in the direction of rotation. On the port side, the thickness noise that is radiated toward the fuselage is reflected toward the ground. On the starboard side, the thickness noise that is radiated toward the fuselage is reflected upward. The thickness noise that is reflected toward the ground on the port side increases the received noise levels on the port side.

SPL plots of the 50-, 63-, and 80-Hz one-third-octave-band levels as a function of slant range for flight path B are given in the appendix. The format of the plots is the same as that in figure 19 to illustrate port/starboard symmetry. Results are given for seven airplane positions: before the overhead position (-2.0, -1.0, and -0.5 sec), at the overhead position (0 sec), and after the overhead position (0.5, 1.0, and 2.0 sec). The corresponding source directivity angles are  $36^\circ$ ,  $56^\circ$ ,  $71^\circ$ ,  $90^\circ$ ,  $109^\circ$ ,  $124^\circ$ , and  $144^\circ$  referenced to the forward direction. The data are plotted to illustrate the airplane deck angle associated with each data point. The data were taken on October 6, 1982, and each data point represents an average of three repeat runs for each of the three deck angles ( $8^\circ$ ,  $5^\circ$ , and  $2^\circ$  nose up). The deck angles were obtained by the corresponding flap settings of 0, 78, and 100 percent. It is difficult to recognize a trend in the results dependent on deck angle. However, the data show an increase in BPF levels on the port side, particularly in the forward direction where directivity angles are less than  $90^\circ$ .

### Review of Results

A flight experiment was conducted to investigate the acoustic propagation of periodic low-frequency noise from a large four-engine, propeller-driven airplane. The experiment consisted of flying the test airplane at altitudes ranging from 15 to 500 m over the end of an 1800-m-long, 22-element microphone array positioned over grass. The microphone array consisted roughly of an equal number of ground-level and 1.2-m microphones. A secondary purpose of the flight experiment was to investigate source installation effects and noise source symmetry. This

second purpose was achieved by flying the test airplane over the middle of the microphone array at a nominal altitude of 100 m. The test airplane was tracked with a laser/radar tracker. Detailed weather information was acquired during the testing periods. The acoustic data were reduced by a one-third-octave-band analysis.

The primary propagation quantities computed from the measured acoustic data were lateral attenuation and ground effects. The excessive scatter observed in the measured results largely obscured the physics of the low-frequency noise propagation. The data scatter made it difficult to identify trends and reach conclusions about the data. Possible causes of the data scatter that were investigated were measurement uncertainty, directivity, microphone height, multisource interference, and source variability.

The observed scatter in the data was greater than that attributable to measurement uncertainty. The weather during the test was judged to be excellent for a flight experiment. Refraction, turbulent scattering, and other propagation anomalies did not play a major role in the observed data scatter. The manner in which lateral attenuation and ground effects are traditionally calculated from measured data depends on source directivity uniformity. In the computational processes for lateral attenuation and ground effects, the difference is taken between two measurements, one underneath and one to the side of the flight path. Computation of lateral attenuation and ground effects using the traditional overhead and sideline measurements can be misleading for highly directional airplane noise sources, such as those on propeller airplanes and rotorcraft. The apparent directivity differences between the sideline and overhead positions for multiengine propeller-driven airplanes may be influenced by multisource interference effects and certainly are influenced by direct/reflected path interference effects if the microphones are positioned above the ground.

The lateral attenuation results showed an increase in scatter and a lowering of lateral attenuation values, including negative values, for the 1.2-m microphones as compared with results from the ground-mounted microphones. The increased scatter and the lowering of values are attributed to the interference pattern caused by the direct and reflected signals received by a microphone positioned above the ground. If both measurements in a lateral attenuation calculation are influenced by interference patterns, the result of the difference operation, particularly for periodic signals, is difficult to interpret.

The lateral attenuation results were more consistent for the ground-mounted microphones than for the 1.2-m microphones, but the ground micro-

phone results still exhibited excessive scatter. The cause of this remaining scatter was attributed to multisource interference and source variability. The source variability was measured in flight with a wingtip boom-mounted microphone. The sound pressure level (SPL) of the blade passage frequency was found to vary more than 9.5 dB over a period of 2 sec. This variability undoubtedly was a large contributor to the observed data scatter.

A trend of increasing lateral attenuation for decreasing elevation angle was discernible for the ground-mounted-microphone data. Lateral attenuation measured in overall sound pressure level (OASPL) was less than 5 dB for elevation angles greater than  $10^\circ$ . For elevation angles less than  $10^\circ$ , the value of lateral attenuation increased to a maximum of 10 dB.

Ground effects results were calculated and compared with a theoretical model. The ground effects predictions formed an upper bound on the measured values of ground effects. The predicted ground effects were less than the measured ground effects. The scatter in the measured results was so large that it became difficult to make detailed comments concerning the theory/measurement comparison.

No consistent installation effects due to varying the test airplane deck angle were discernible. Again, the large amount of scatter in the data made data interpretation difficult. The test airplane propellers rotated in a counterclockwise direction when viewed from the front. The measured results showed a noise asymmetry. The measured ground noise levels were larger on the port side of the test airplane than on the starboard side, particularly for the blade passage frequency. The asymmetry was attributed to fuselage shielding.

The data scatter in the measured acoustic data has been shown to be largely a characteristic of the noise sources of the test airplane. The values of lateral attenuation and ground effects calculated from the measured data are valid for the test airplane within the definitions of lateral attenuation and ground effects used in this paper. The scatter in the results makes trend identification difficult. Different concepts of lateral attenuation and ground effects may be needed for airplanes dominated by periodic low-frequency noise, particularly for multiengine propeller airplanes and rotorcraft.

## References

1. *Prediction Method for Lateral Attenuation of Airplane Noise During Takeoff and Landing*. AIR 1751, Soc. Automotive Engineers, Inc., Mar. 30, 1981.

2. *Estimation of One-Third-Octave-Band Lateral Attenuation of Sound From Jet-Propelled Airplanes.* AIR 1906, Soc. Automotive Engineers, Inc., Oct. 1985.
3. Sutherland, Louis C.; and Brown, Ron: *Static Tests of Excess Ground Attenuation at Wallops Flight Center.* NASA CR-3435, 1981.
4. Willshire, William L., Jr.; and Nystrom, Paul A.: *Investigation of Effects of Microphone Position and Orientation on Near-Ground Noise Measurements.* NASA TP-2004, 1982.
5. *Method for the Calculation of the Absorption of Sound by the Atmosphere.* ANSI S1.26-1978 (ASA 23-1978), American Natl. Standards Inst., Inc., June 23, 1978.
6. Willshire, William L., Jr.: *Ground Effects on Aircraft Noise for a Wide-Body Commercial Airplane.* *J. Aircr.*, vol. 20, no. 4, Apr. 1983, pp. 345-349.
7. Pao, S. Paul; Wenzel, Alan R.; and Oncley, Paul B.: *Prediction of Ground Effects on Aircraft Noise.* NASA TP-1104, 1978.

Table I. Test Matrix

Airplane altitude, m	Flight path	Flap angle setting, percent	Number of runs
15	A	78	9
30	A	78	6
60	A	78	6
120	A	78	7
240	A	78	8
480	A	78	4
90	B	0	3
90	B	78	10
90	B	100	3
90	A	0	1
Total . . . . .			57

Table II. Microphone Coordinates

Microphone	Nominal height, m (a)	Coordinates		
		X, m	Y, m	Z, m
1	0.0	-128.5	55.3	-0.7
2	1.2	-128.5	53.3	.5
3	0.0	-326.6	56.6	-.5
4	1.2	-326.6	54.6	.7
5	0.0	-433.3	56.6	-.6
6	1.2	-433.3	54.6	.6
7	0.0	-738.1	71.9	-.2
8	1.2	-738.1	69.9	1.0
9	0.0	-936.2	55.3	-1.0
10	1.2	-936.2	53.3	.2
11	0.0	-1164.8	81.2	-2.3
12	1.2	-1164.8	79.3	-1.1
13	0.0	-1347.7	81.2	-1.6
14	1.2	-1347.7	79.3	-.4
15	0.0	-1561.1	81.2	-1.4
16	1.2	-1561.1	79.3	-.2
17	0.0	-1759.2	81.2	-2.2
18	1.2	-1759.2	79.3	-1.0
19	0.0	0.0	0.0	0.0
20	0.0	48.8	75.2	0.0
21	0.0	65.5	-113.5	0.0
22	1.2	67.8	-117.5	1.2

<sup>a</sup>0: microphone at ground level; 1.2: microphone 1.2 m above ground.

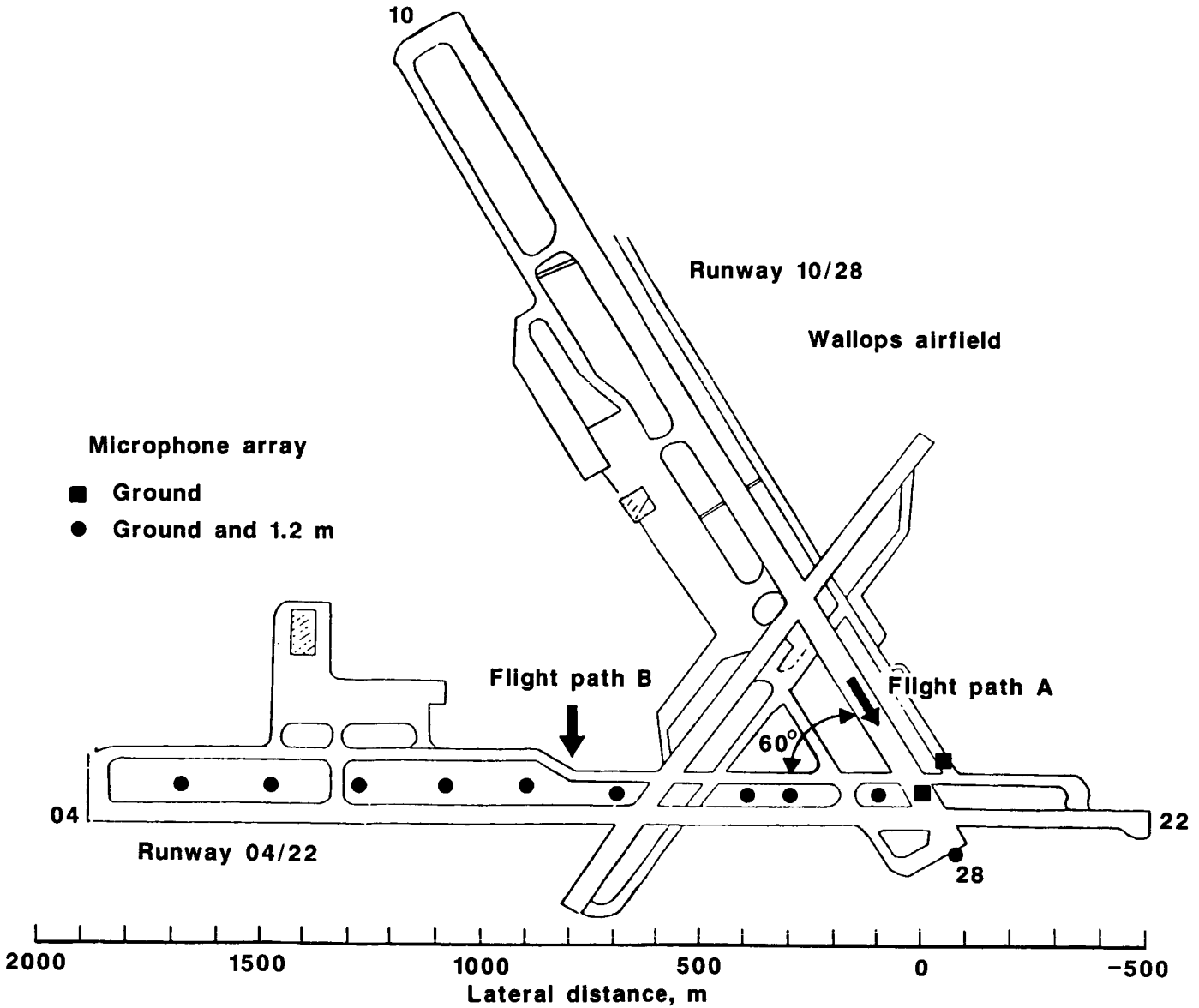
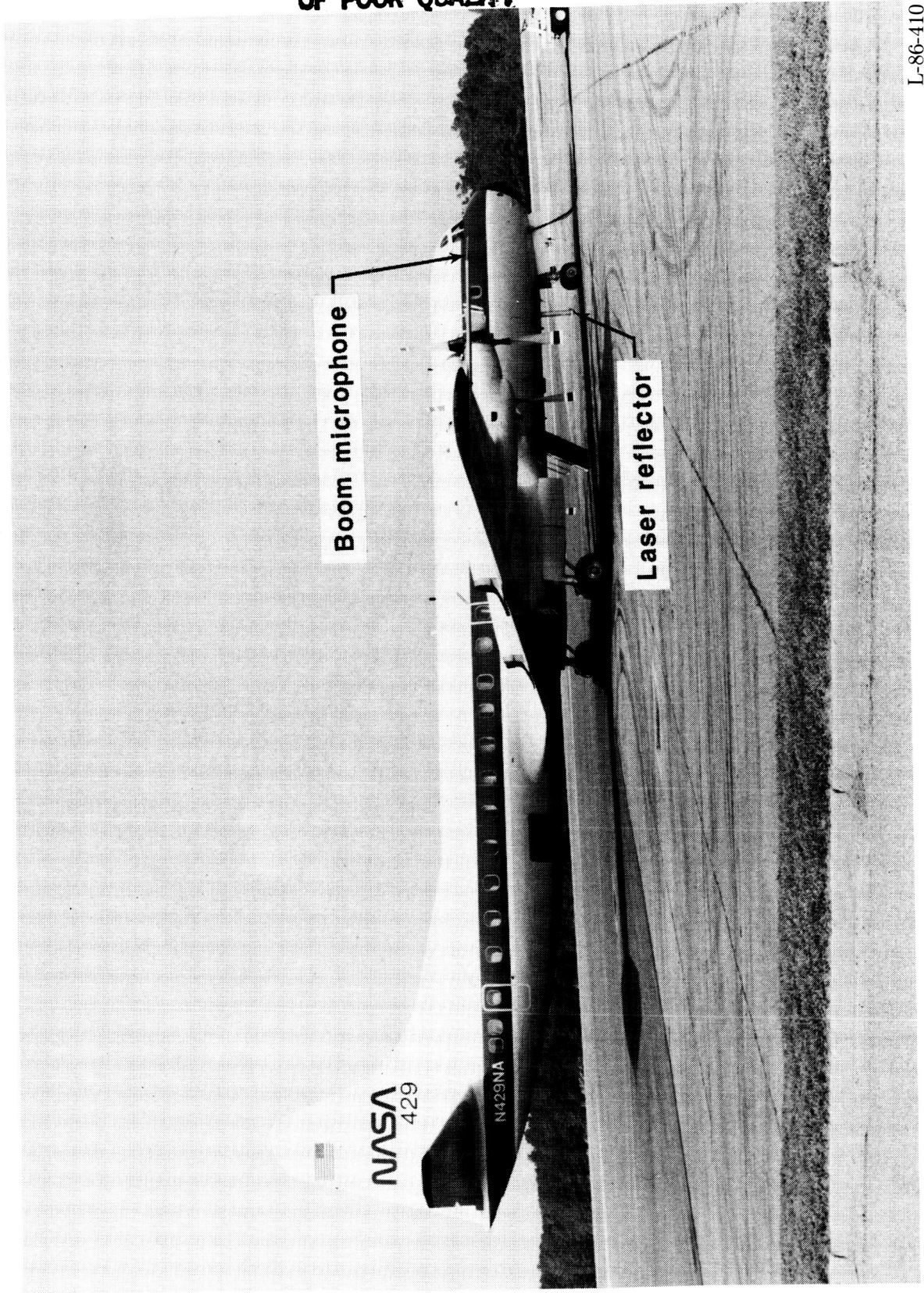


Figure 1. Microphone layout and flight paths.

ORIGINAL PAGE IS  
OF POOR QUALITY



L-86-410

Figure 2. Photograph of test airplane.

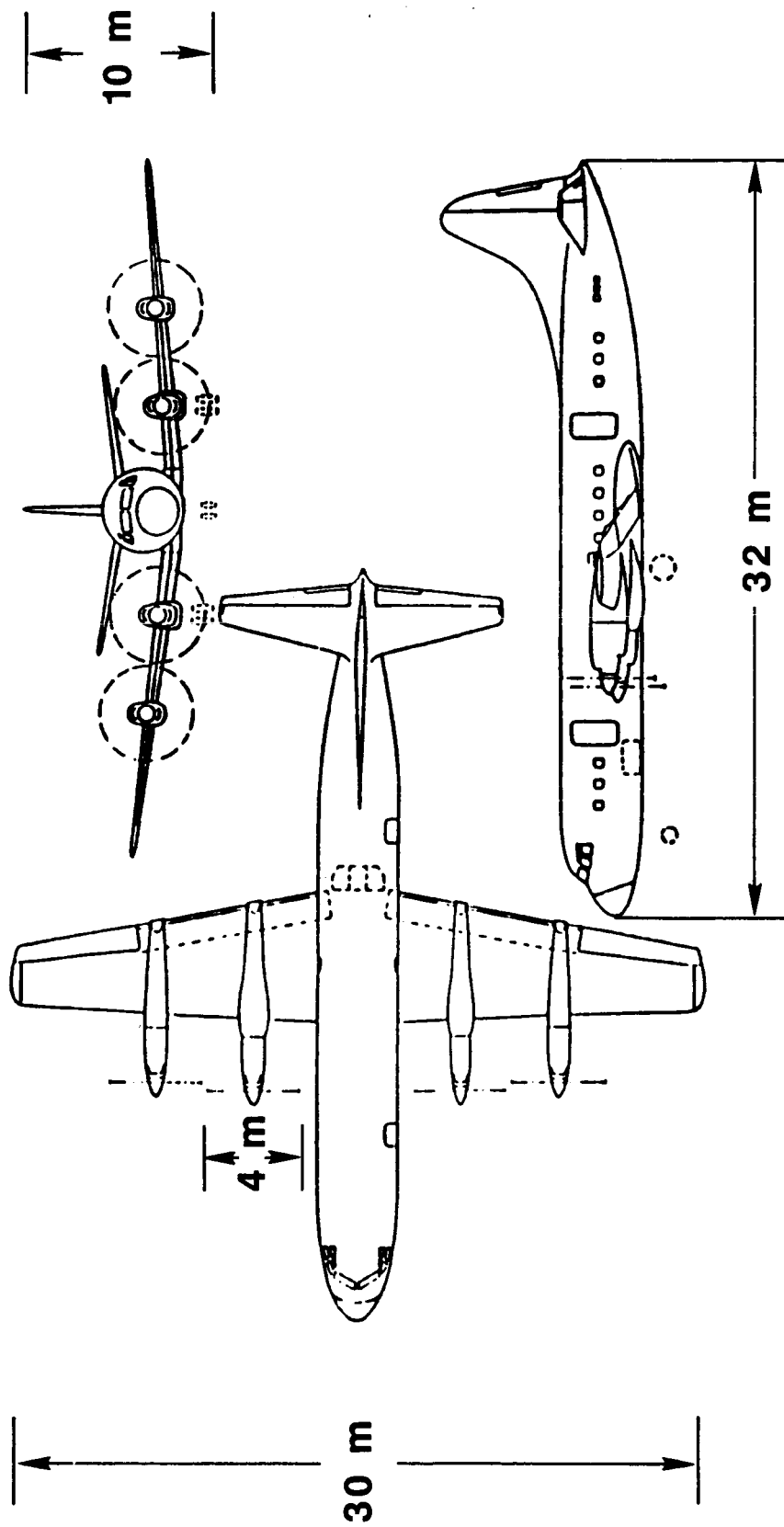


Figure 3. Three-view drawing of test airplane.

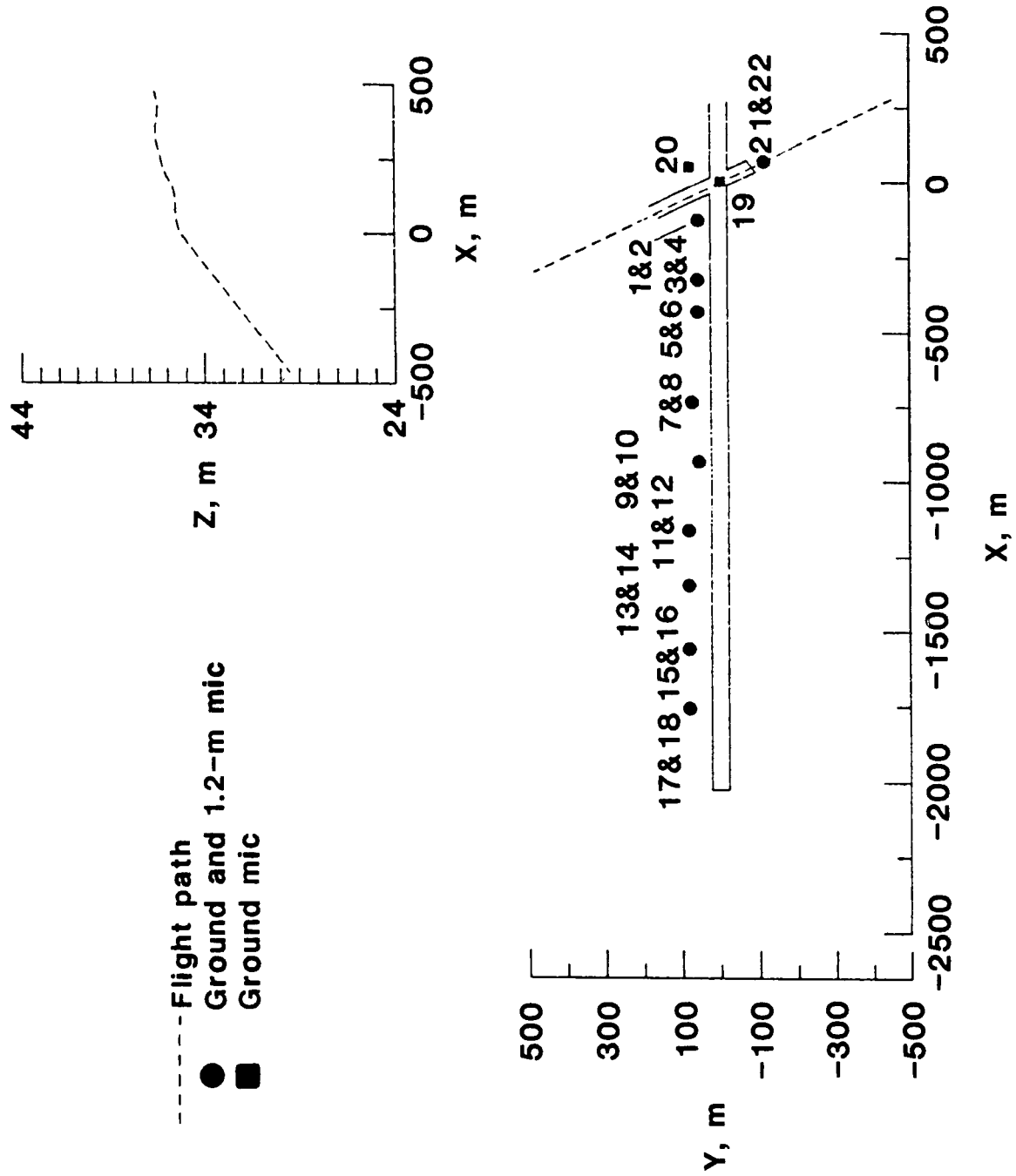


Figure 4. Tracking data for flight path A.

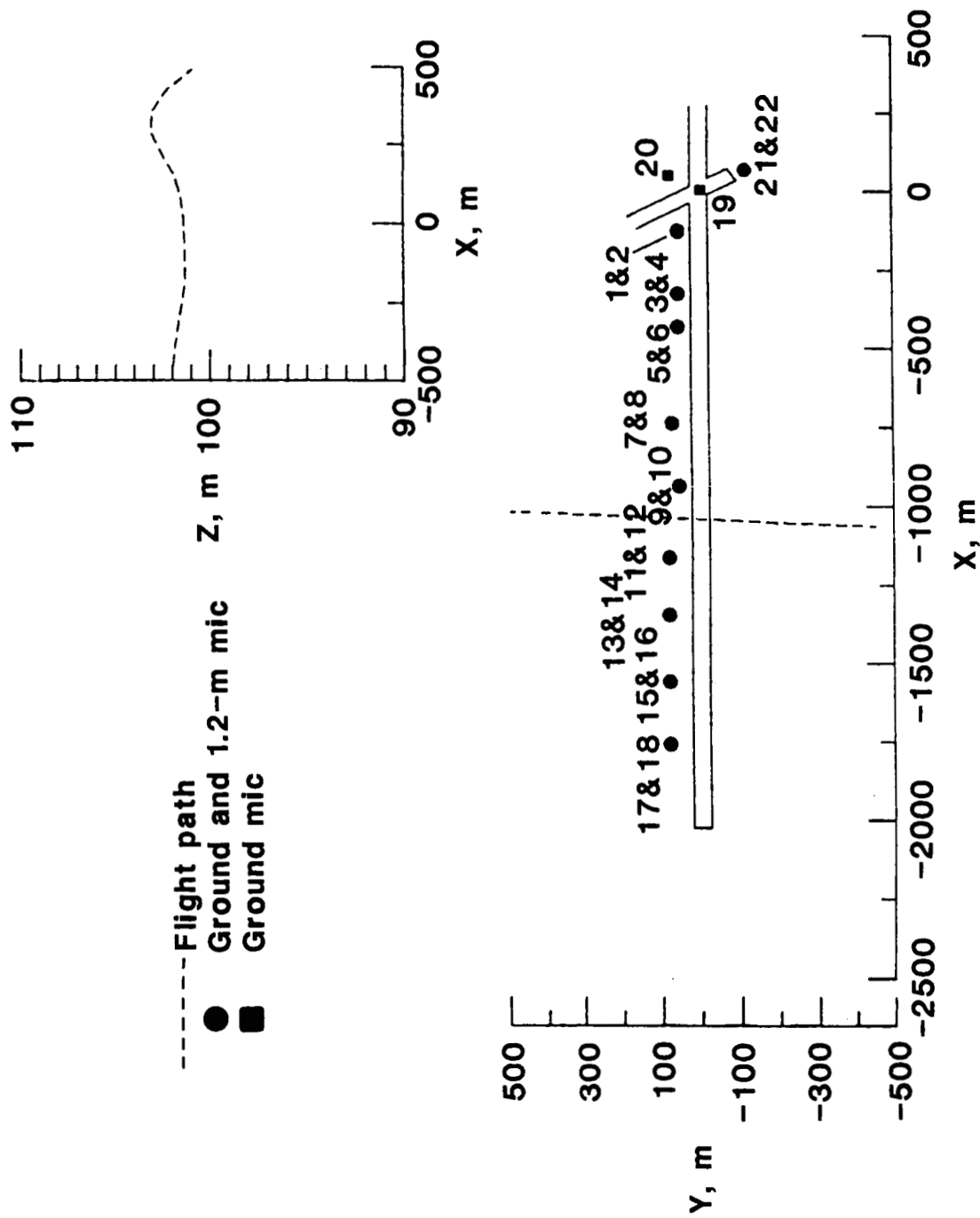
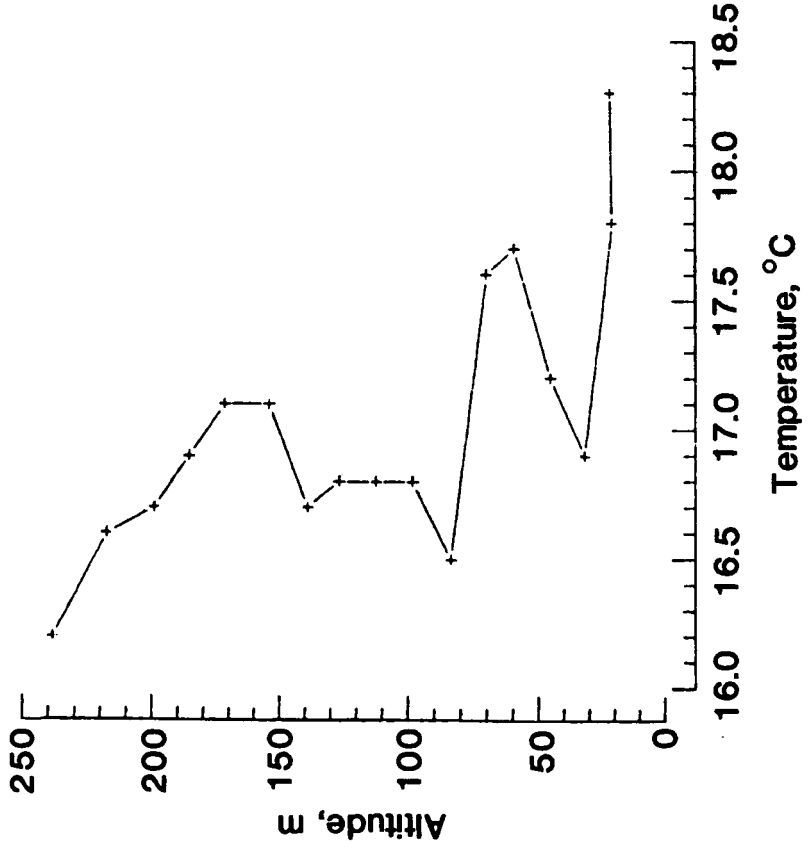
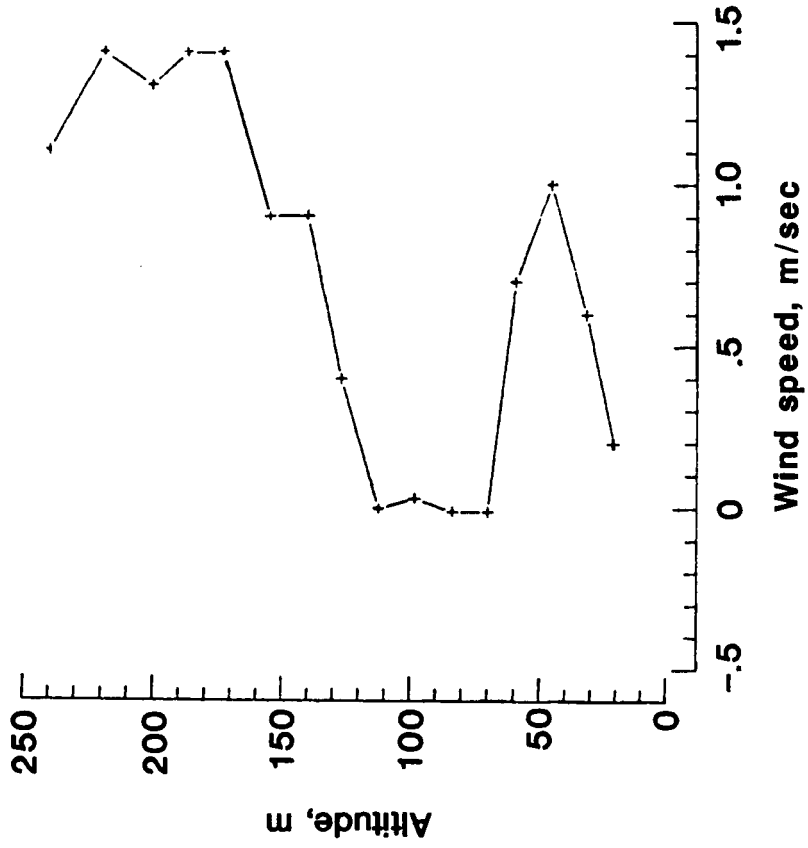


Figure 5. Tracking data for flight path B.

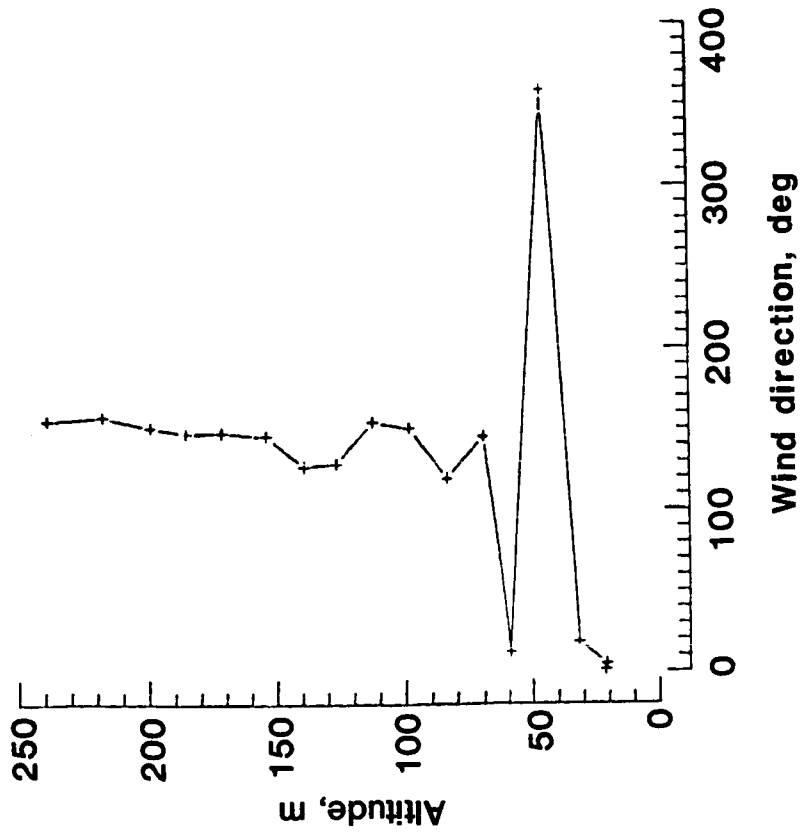


(a) Temperature profile.

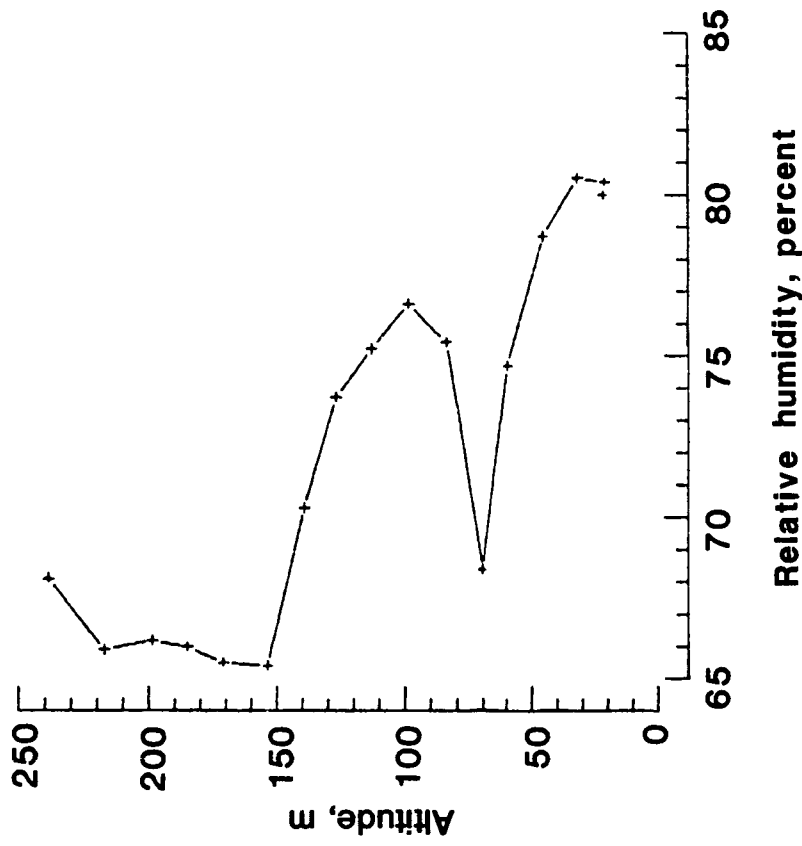


(b) Wind speed profile.

Figure 6. Weather balloon data measured on October 3, 1982.

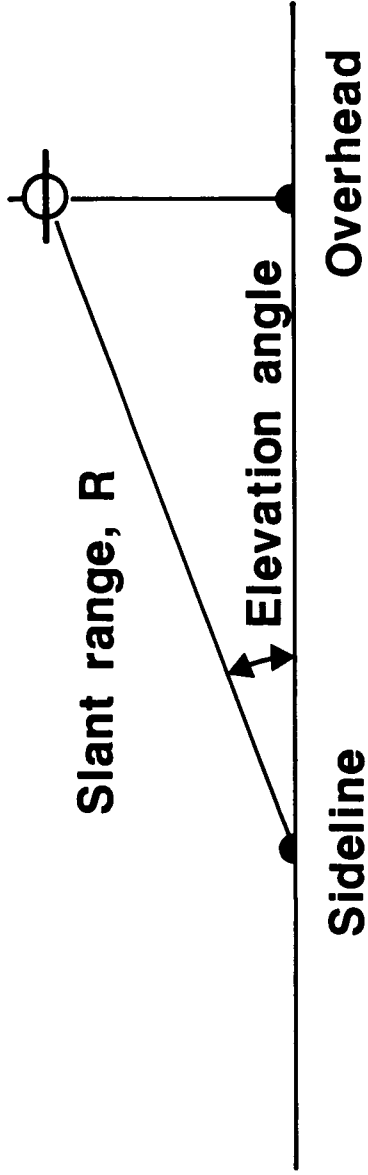


(c) Wind direction profile.



(d) Relative humidity profile.

Figure 6. Concluded.



$$\text{Lateral attenuation} = (\text{Overhead})_R - (\text{Sideline})_R$$

$$\text{Ground effects} = (\text{Sideline})_R - (\text{Free field})_R$$

Figure 7. Definitions of lateral attenuation, ground effects, slant range, and elevation angle.

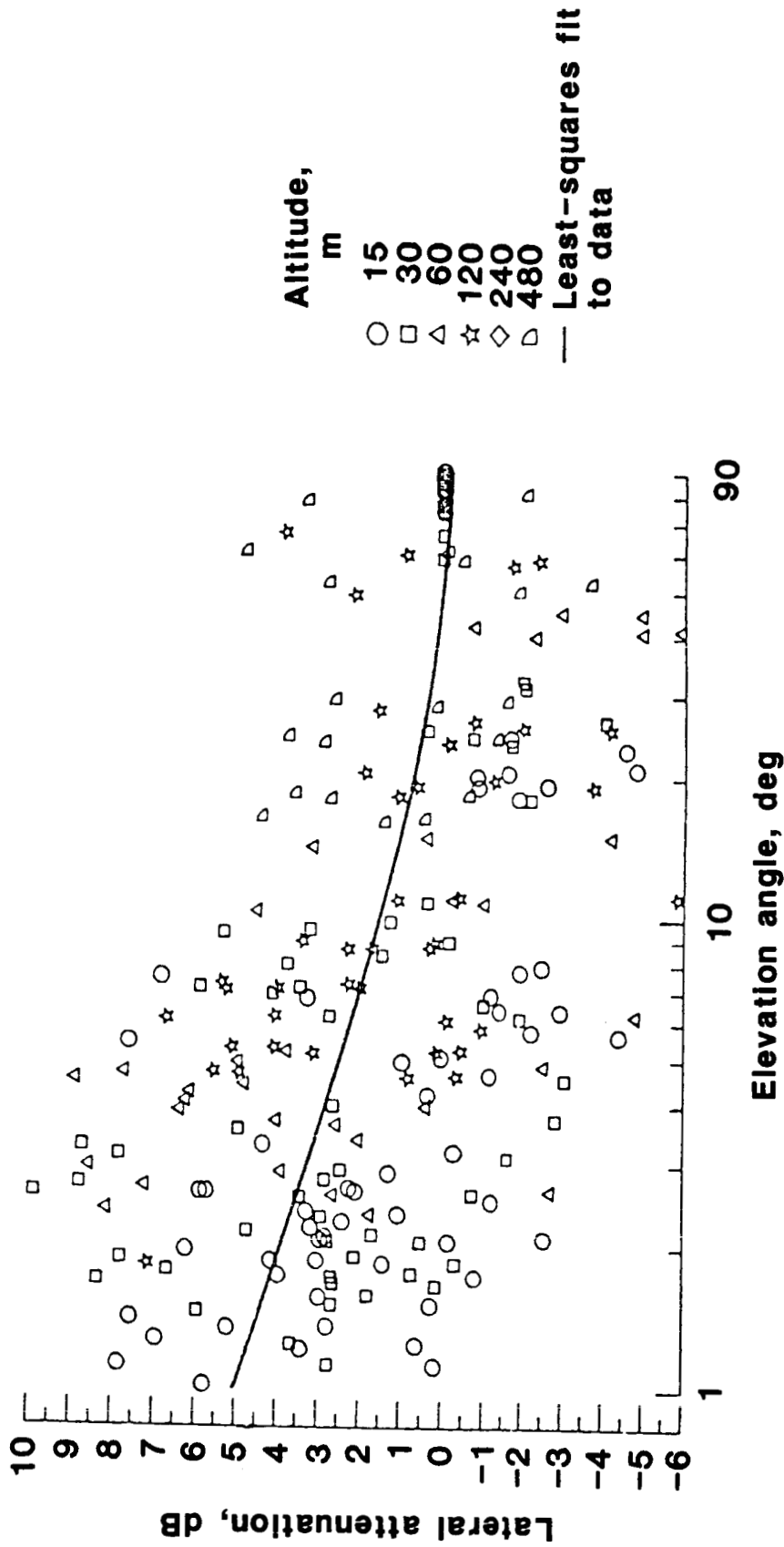


Figure 8. Lateral attenuation results in OASPL for 1.2-m microphones for selected runs on flight path A beginning at an altitude of 15 m. Data symbols denote 1/2-sec averaged data.

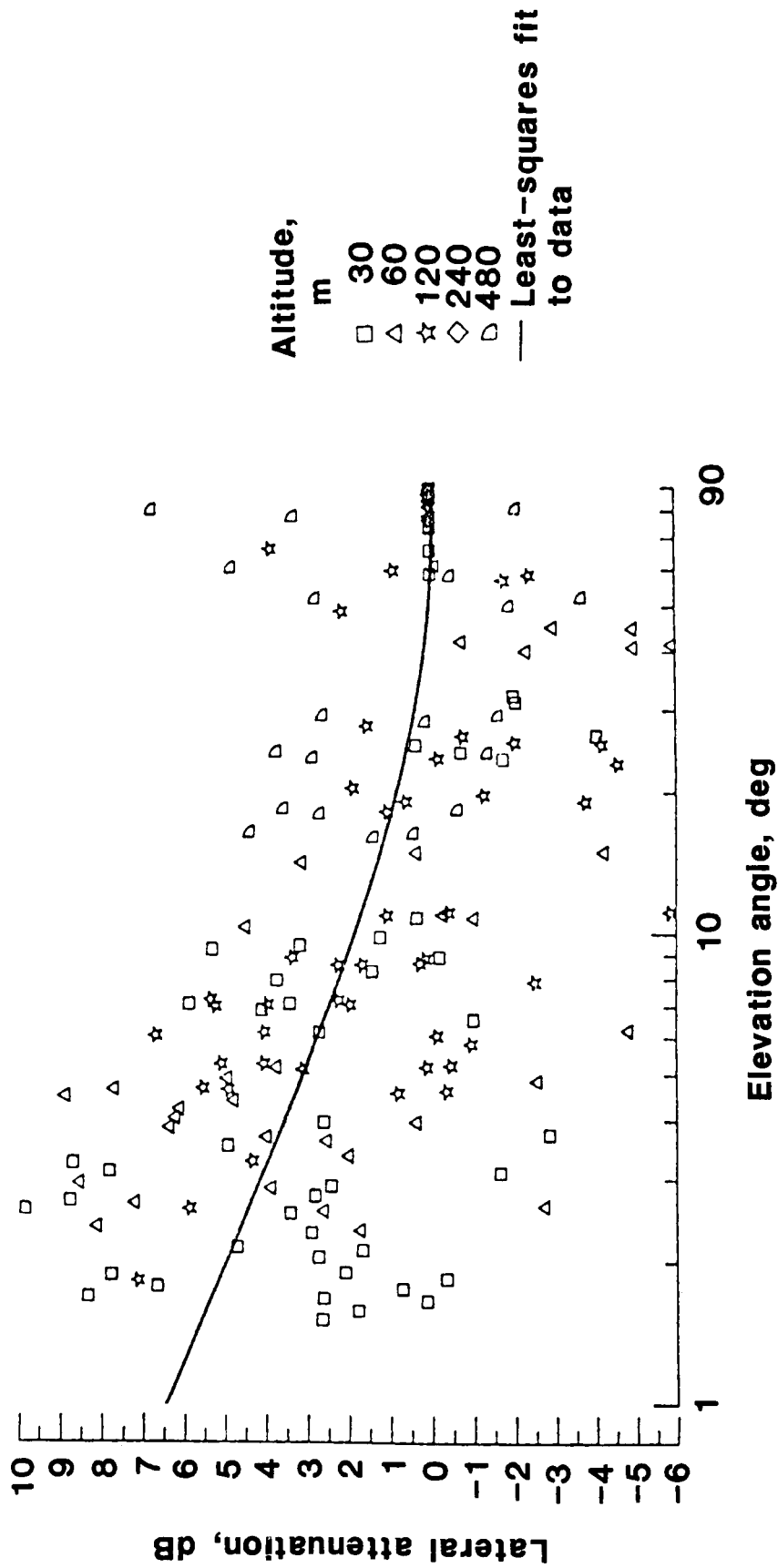
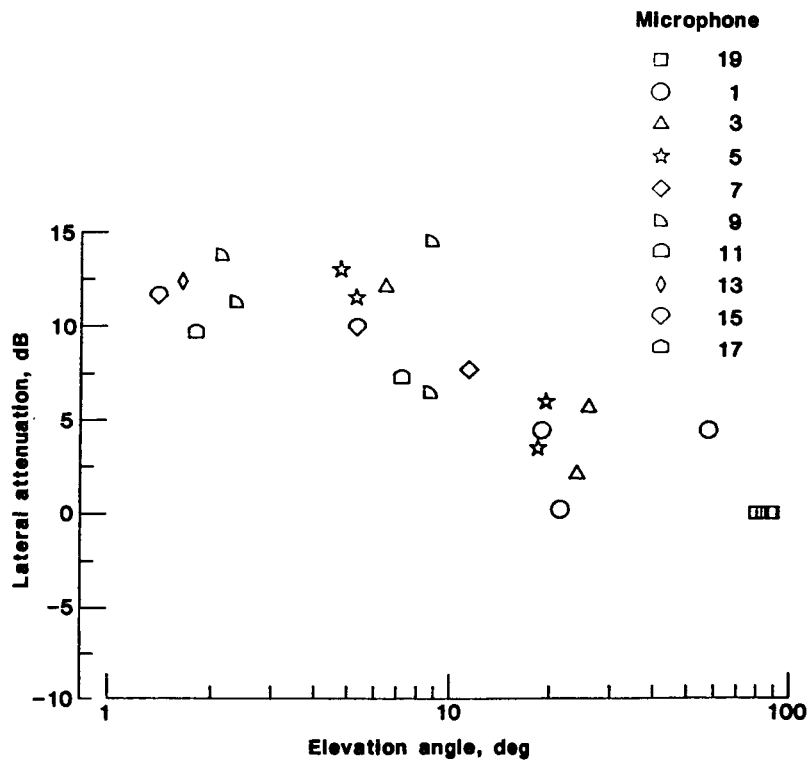
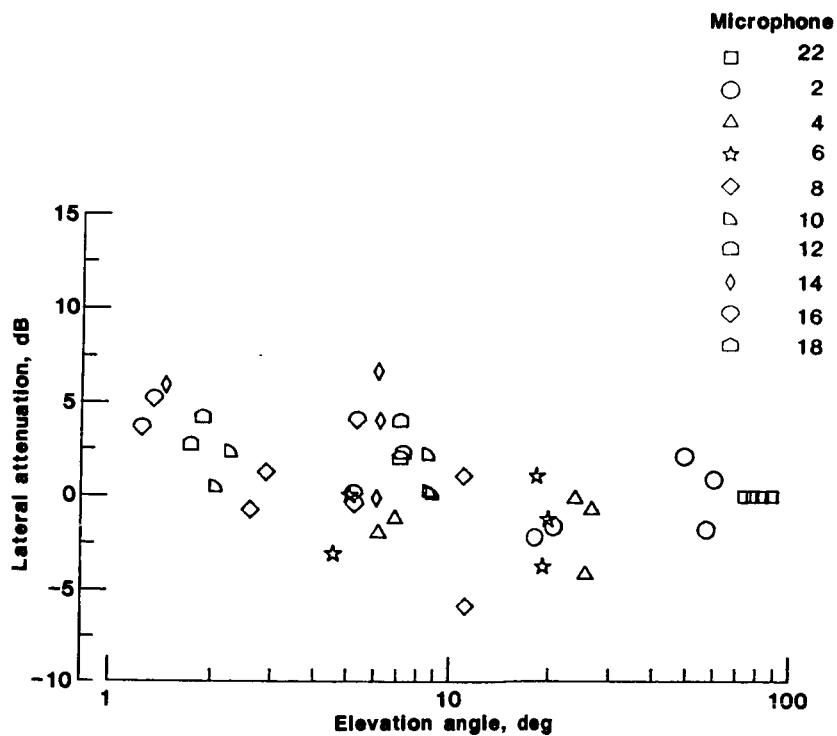


Figure 9. Lateral attenuation results in OASPL for 1.2-m microphones for selected runs on flight path A at altitudes greater than 15 m. Data symbols denote 1/2-sec averaged data.

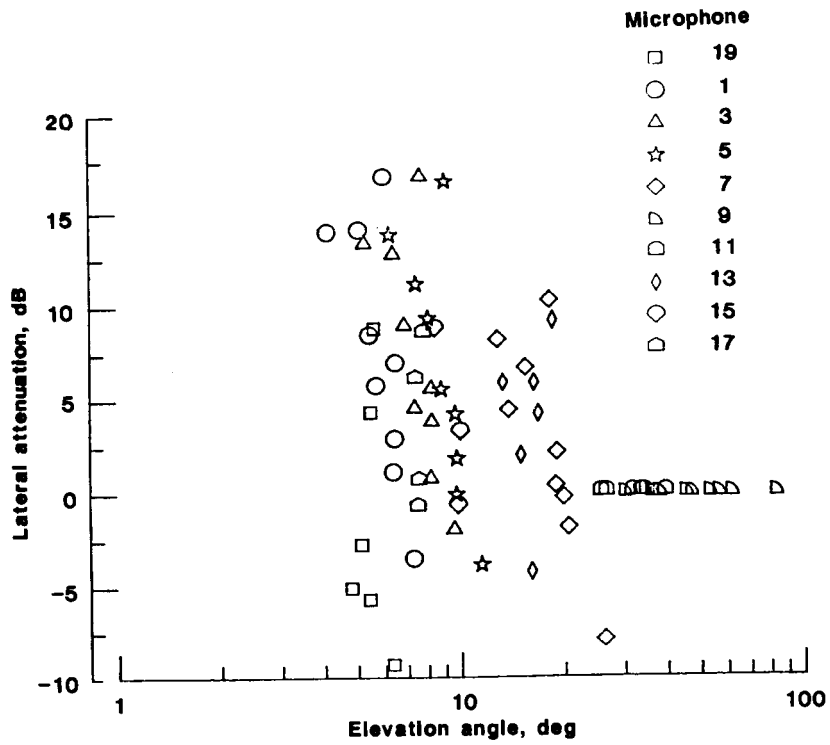


(a) Ground-mounted microphones.

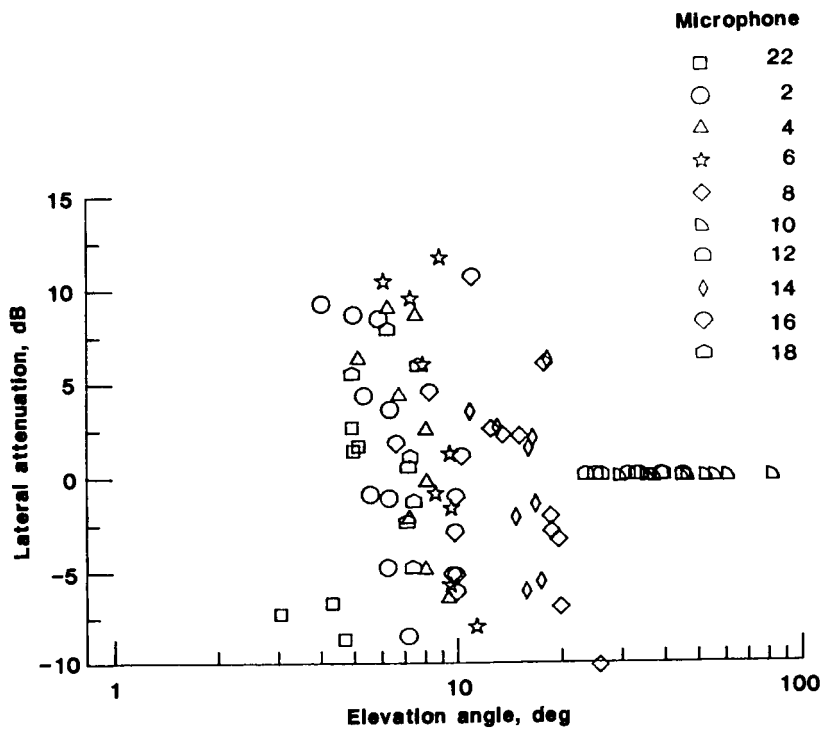


(b) 1.2-m microphones.

Figure 10. Lateral attenuation results in OASPL for selected runs on flight path A. Data symbols denote 1/2-sec averaged data.

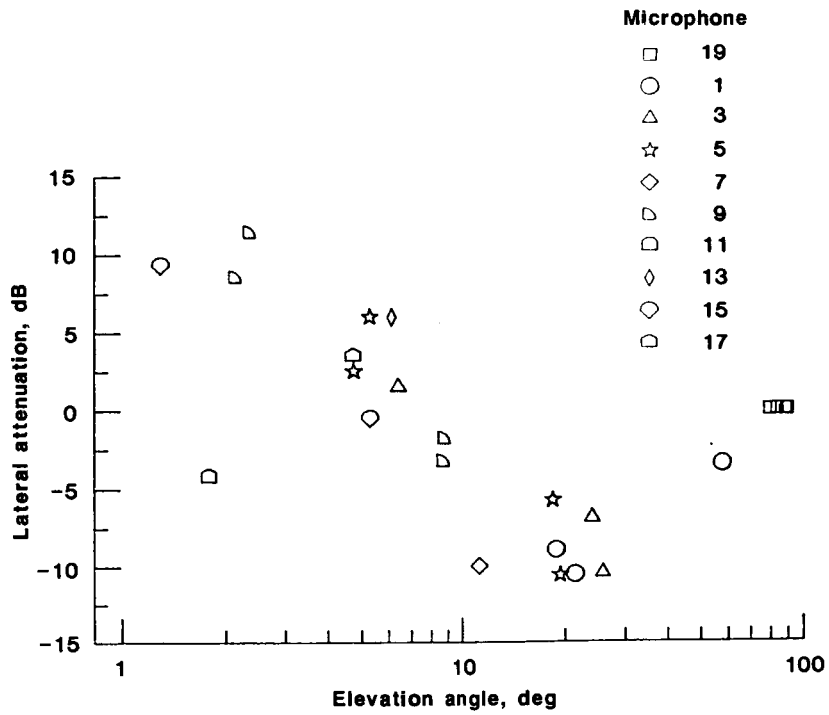


(a) Ground-mounted microphones.

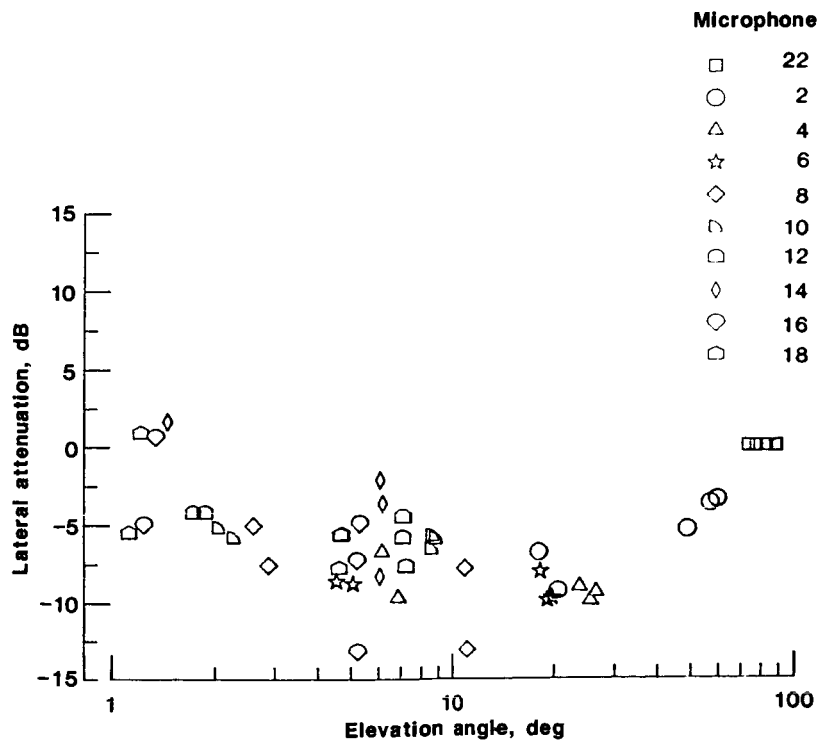


(b) 1.2-m microphones.

Figure 11. Lateral attenuation results in OASPL for selected runs on flight path B. Data symbols denote 1/2-sec averaged data.

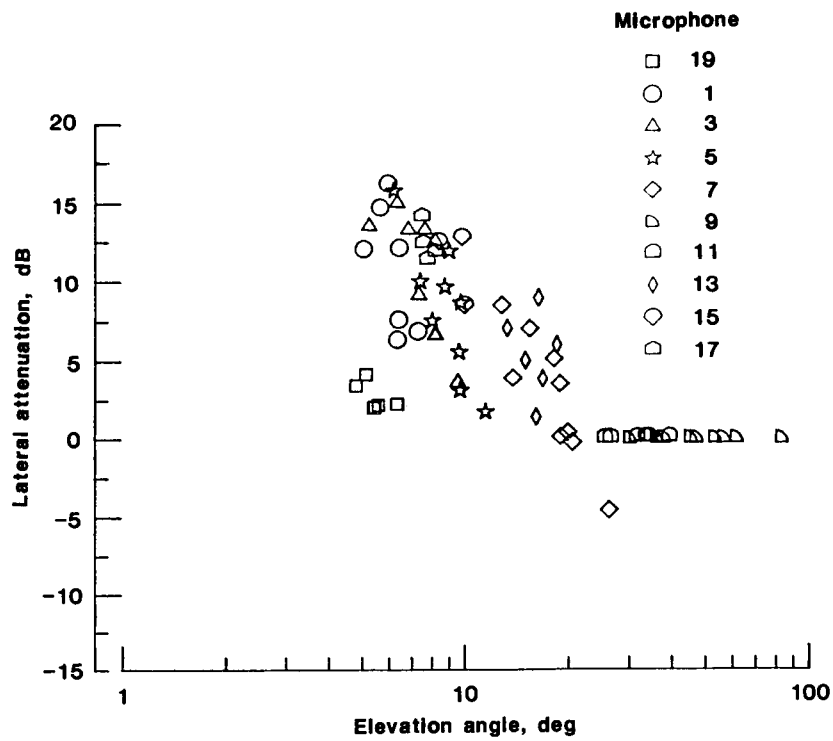


(a) Ground-mounted microphones.

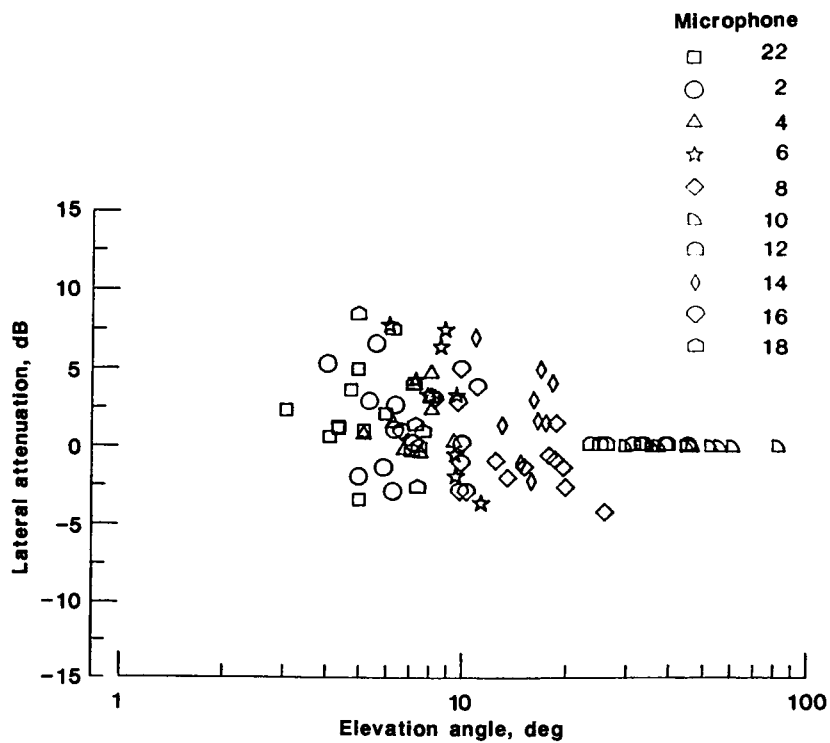


(b) 1.2-m microphones.

Figure 12. Lateral attenuation results in A-weighted SPL for selected runs on flight path A. Data symbols denote  $\frac{1}{2}$ -sec averaged data.

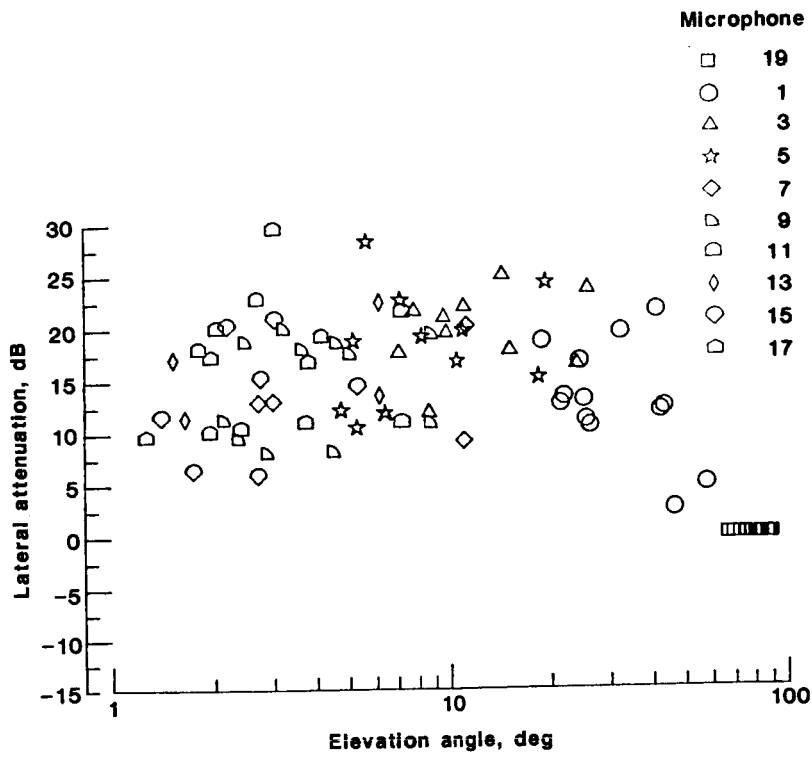


(a) Ground-mounted microphones.

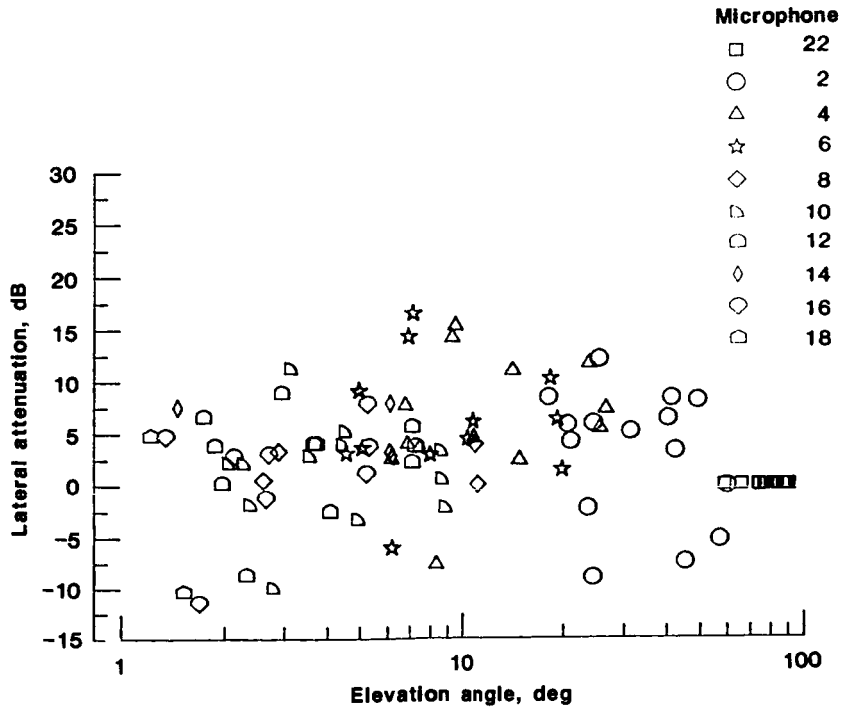


(b) 1.2-m microphones.

Figure 13. Lateral attenuation results in A-weighted SPL for selected runs on flight path B. Data symbols denote 1/2-sec averaged data.

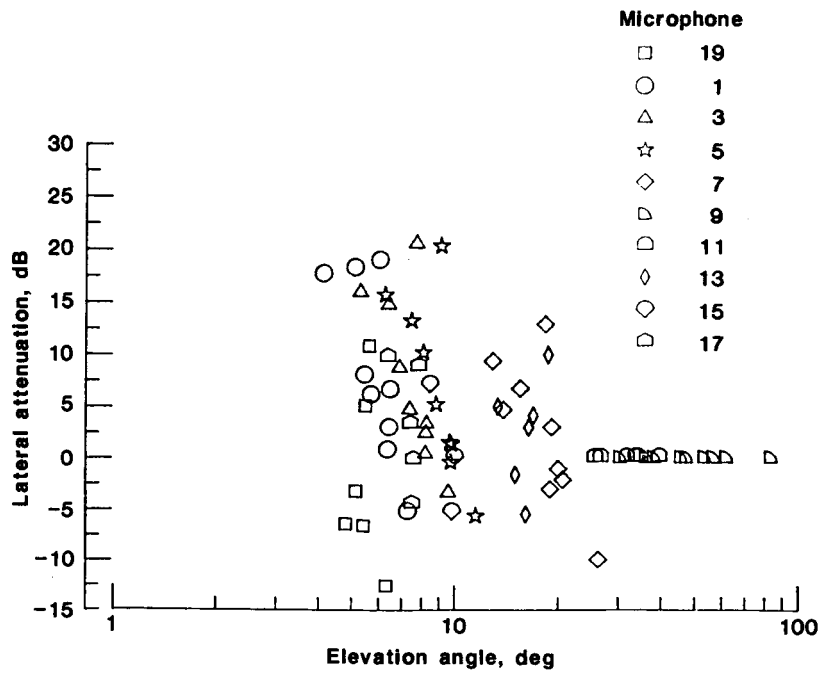


(a) Ground-mounted microphones.

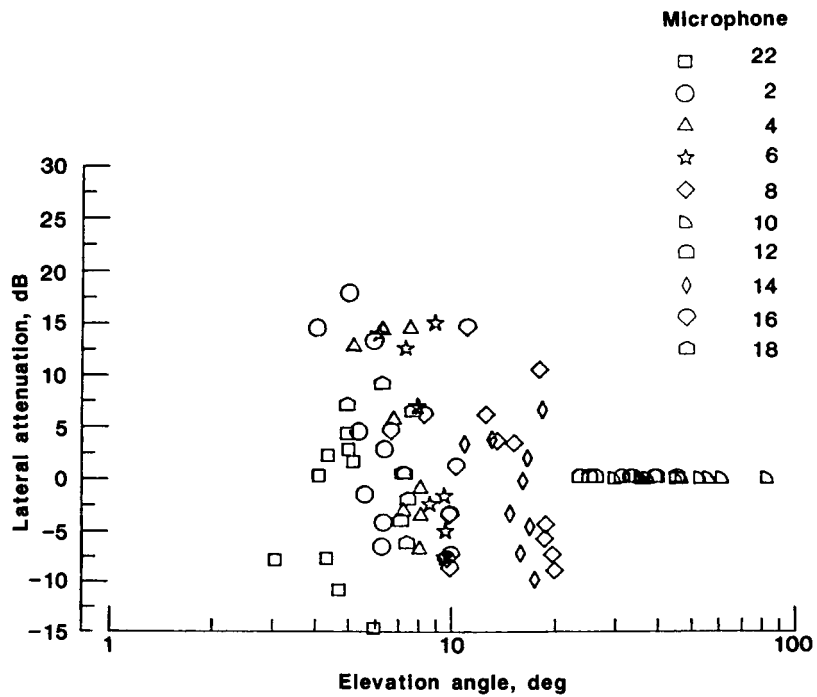


(b) 1.2-m microphones.

Figure 14. Lateral attenuation results in BPF SPL for selected runs on flight path A. Data symbols denote  $\frac{1}{2}$ -sec averaged data.



(a) Ground-mounted microphones.



(b) 1.2-m microphones.

Figure 15. Lateral attenuation results in BPF SPL for selected runs on flight path B. Data symbols denote 1/2-sec averaged data.

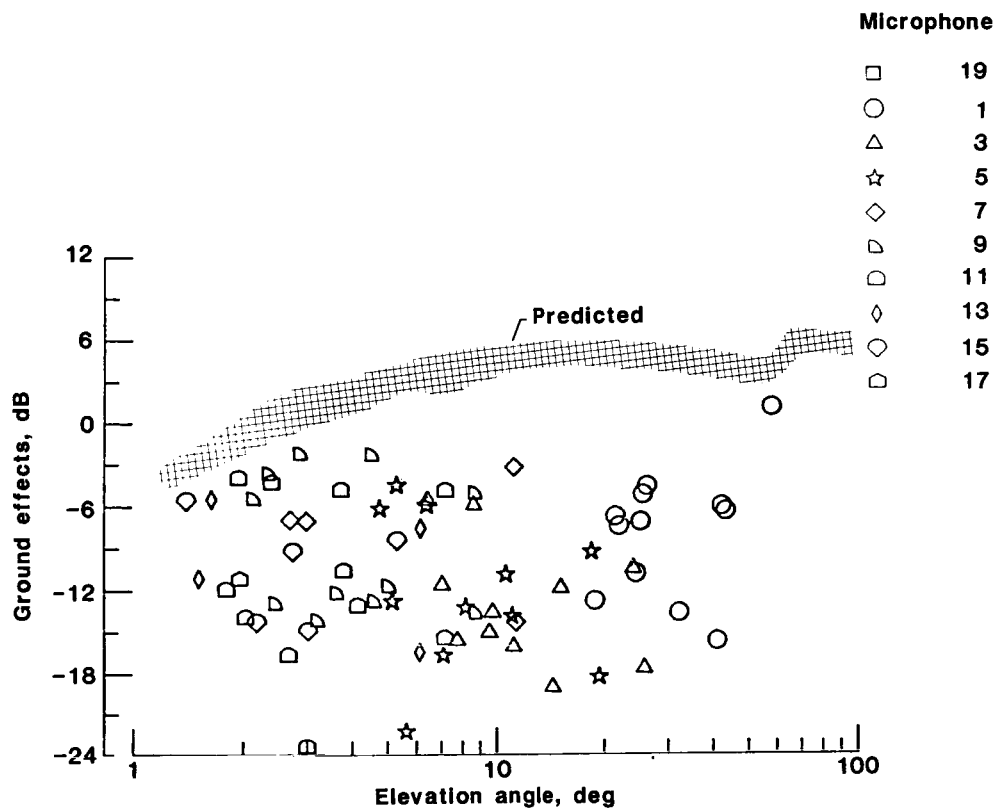


Figure 16. Ground effects results in BPF SPL with predictions for ground-mounted microphones for flight path A. Data symbols denote  $\frac{1}{2}$ -sec averaged data.

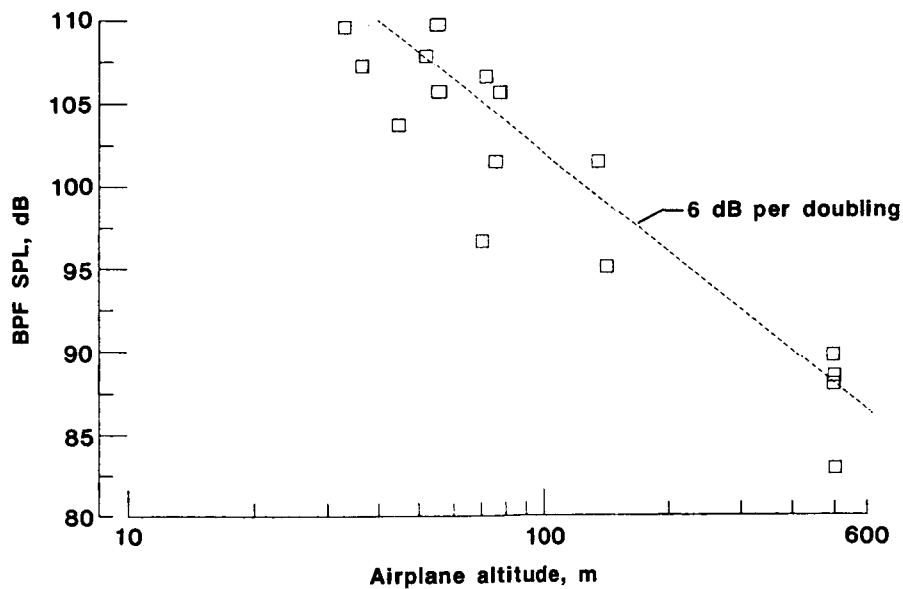
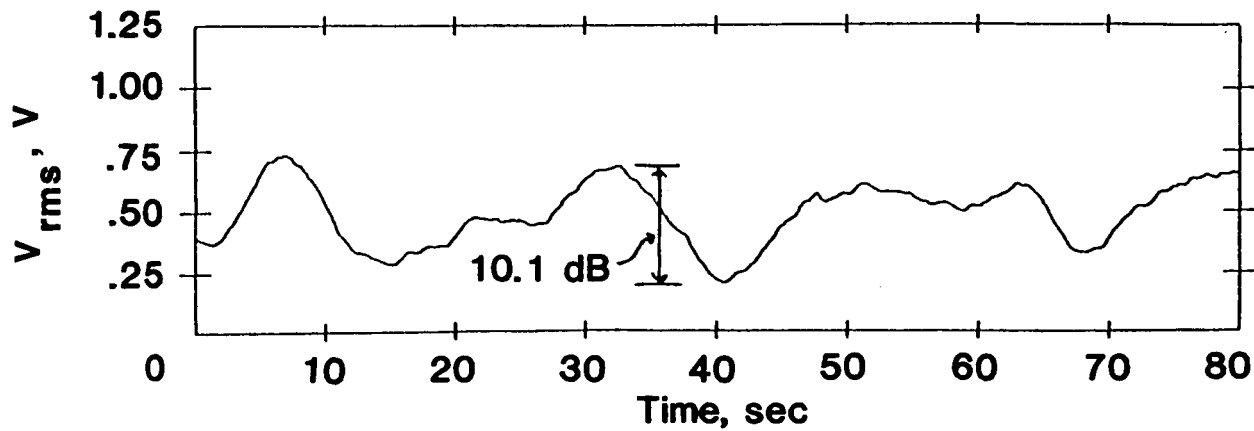
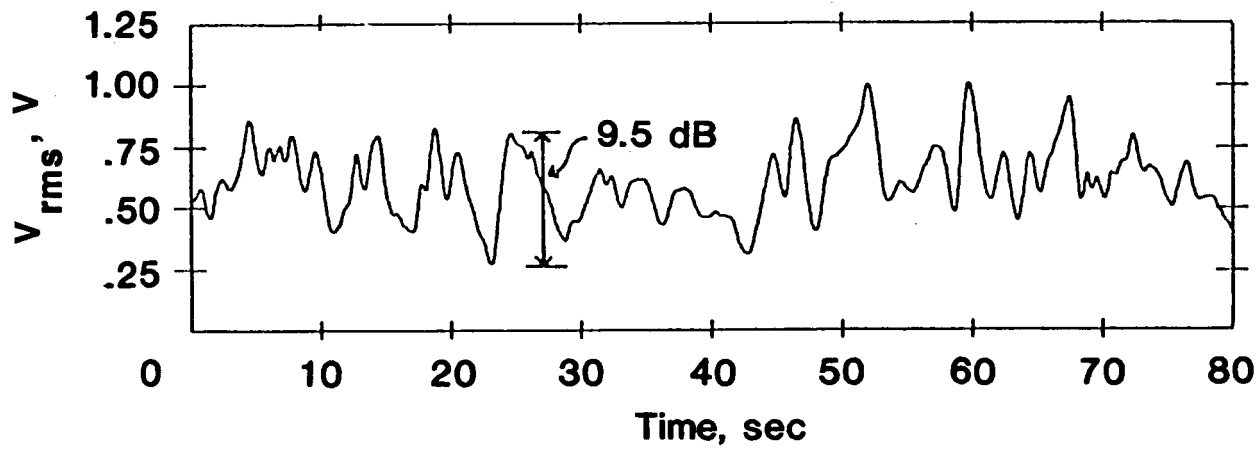


Figure 17. BPF SPL versus airplane altitude for ground-mounted microphone underneath flight path. Data symbols denote  $\frac{1}{2}$ -sec averaged data.



(a) 500-m altitude.



(b) 15-m altitude.

Figure 18. Time histories of root-mean-square signal for wingtip boom-mounted microphone.

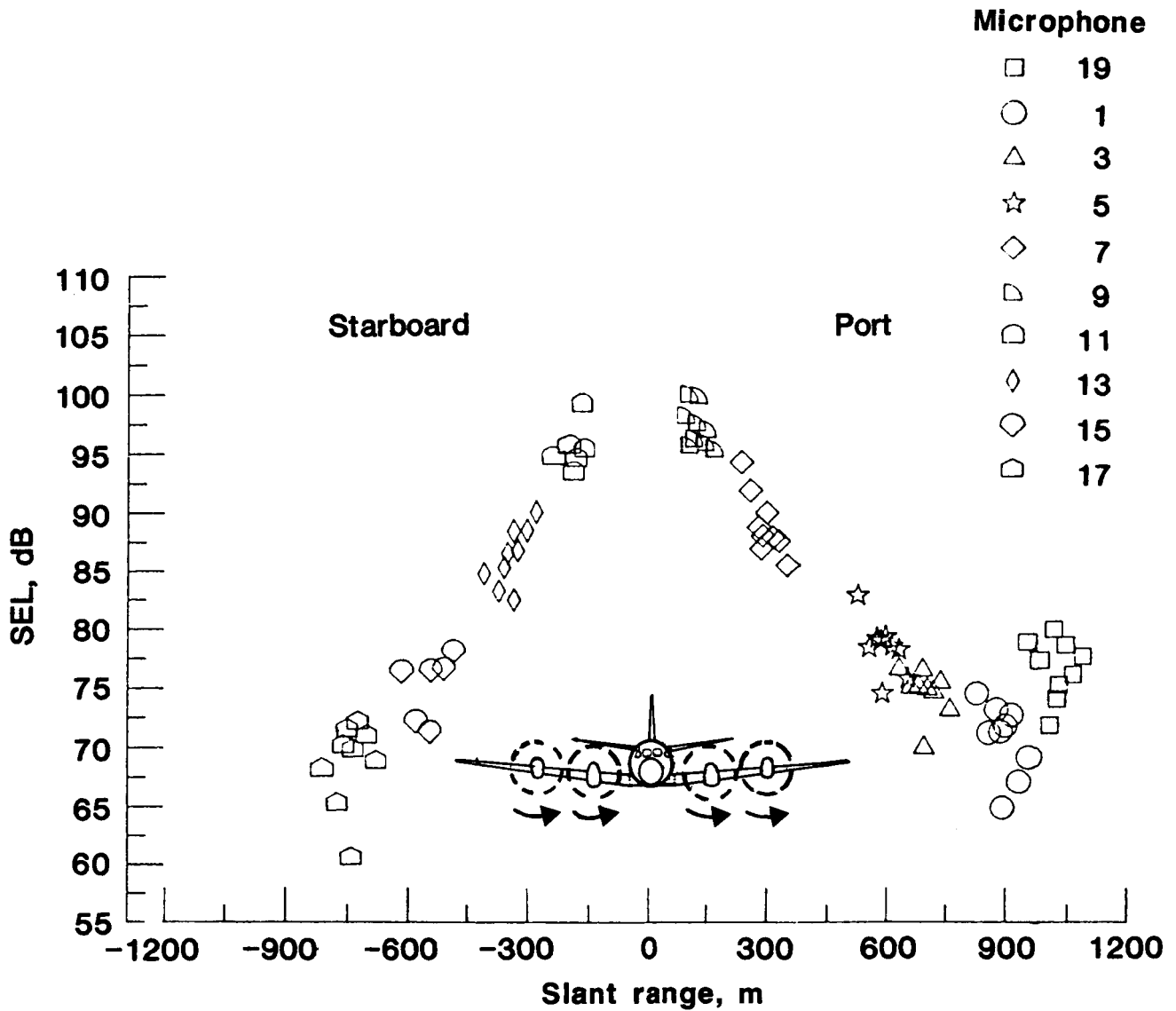


Figure 19. Results of SEL versus slant range for ground-mounted microphones for flight path B.

## Appendix

### Results of One-Third-Octave-Band Noise Source Symmetry

Plots of the sound pressure level (SPL) of the 50-, 63-, and 80-Hz one-third-octave-band levels as a function of slant range for flight path B are given in figures A1 to A7. The purpose of the plots is to illustrate port/starboard symmetry in the format of SPL versus slant range to the right and left of the test airplane ground track. Results are given for seven airplane positions. The positions are -2.0, -1.0, -0.5, 0, 0.5, 1.0, and 2.0 sec from the overhead position, and the corresponding source directivity

angles are 36°, 56°, 71°, 90°, 109°, 124°, and 144° referenced to the forward direction. The data are plotted to illustrate the deck angle associated with each data point. The deck angle was varied by changing the flap settings. The nominal values of deck angle flown were 8°, 5°, and 2° nose up, and the corresponding flap angle settings were 0, 78, and 100 percent. The data were taken on October 6, 1982, and each data point represents an average of three repeat runs for each of the three deck angles. It is difficult to recognize a trend in the results dependent on deck angle. However, the data show an increase in BPF levels on the port side, particularly in the forward direction where directivity angles are less than 90°.

**PRECEDING PAGE BLANK NOT FILMED**

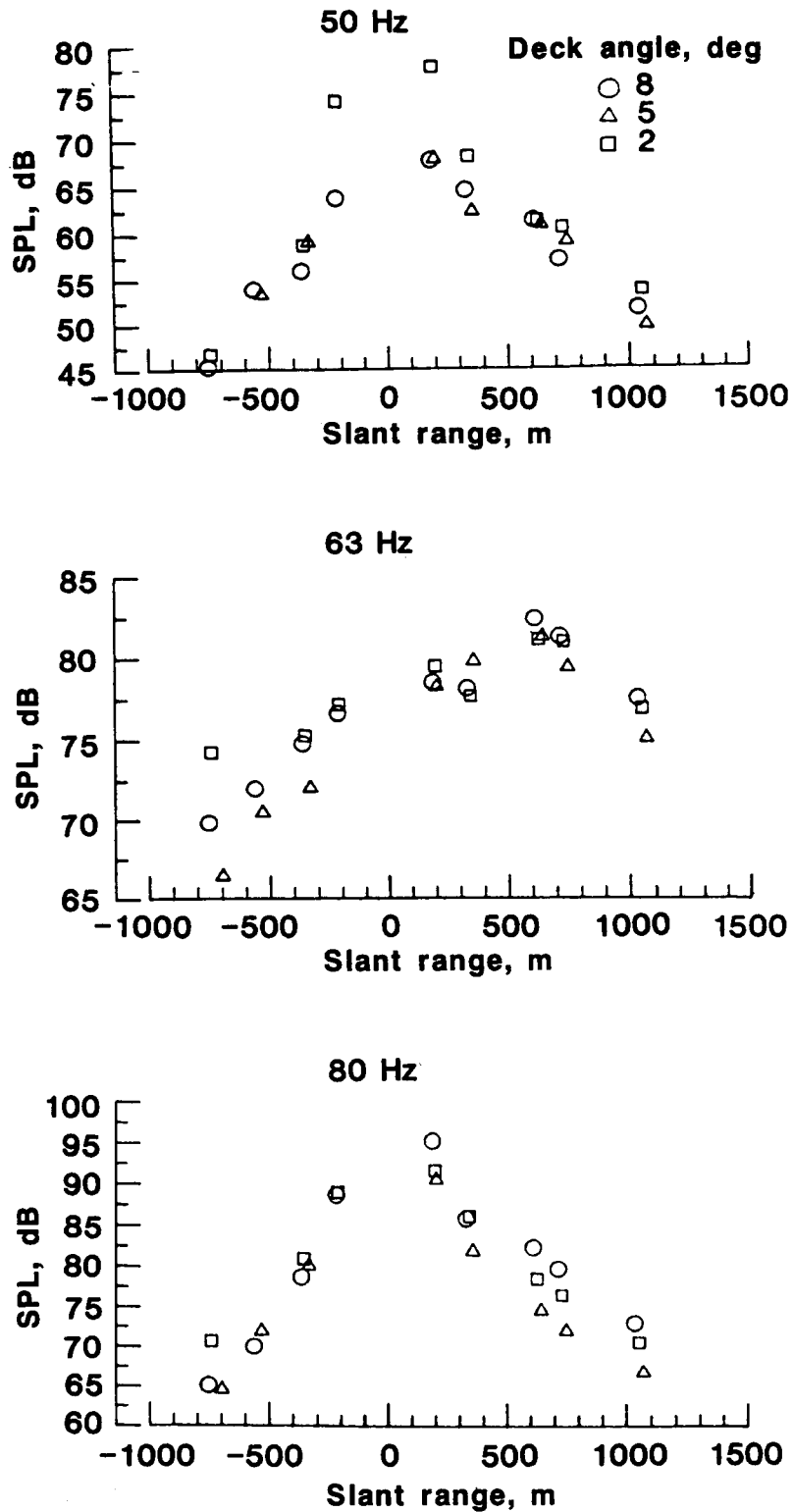


Figure A1. Results of one-third-octave-band SPL versus slant range for flight path B 2.0 sec before overhead position. Source directivity angle,  $36^\circ$ ; data symbols denote  $\frac{1}{2}$ -sec averaged data.

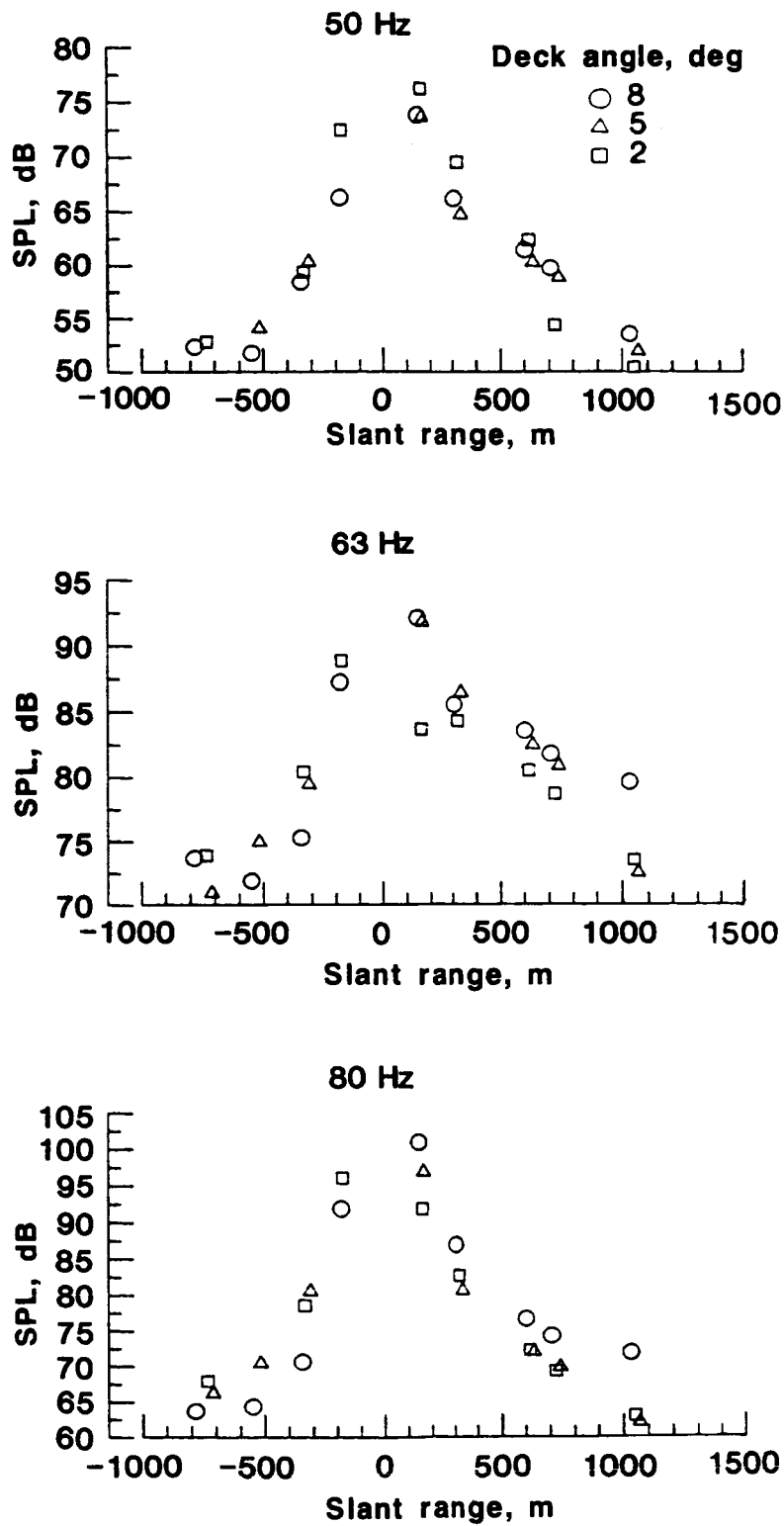


Figure A2. Results of one-third-octave-band SPL versus slant range for flight path B 1.0 sec before overhead position. Source directivity angle,  $56^\circ$ ; data symbols denote  $\frac{1}{2}$ -sec averaged data.

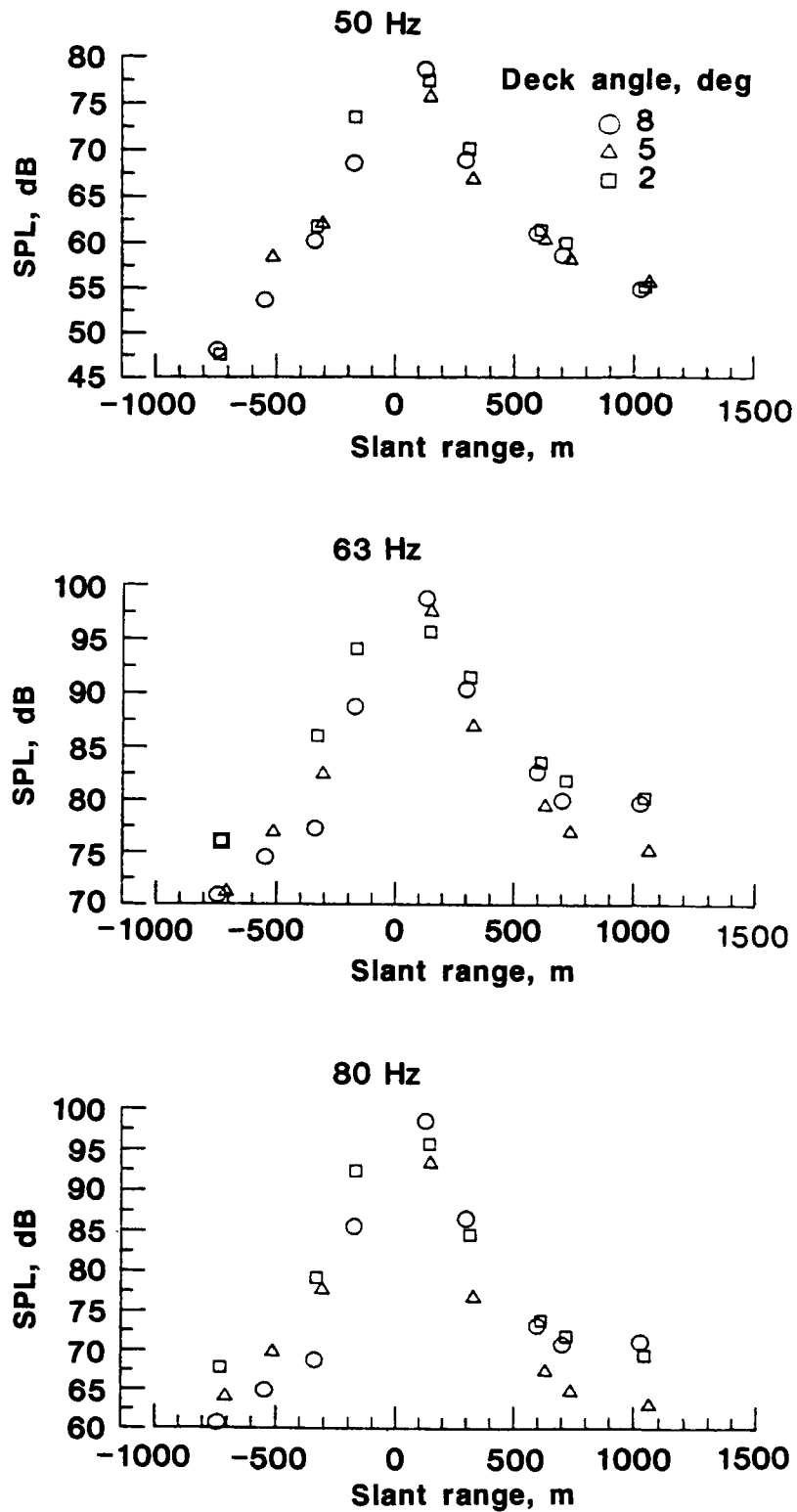


Figure A3. Results of one-third-octave-band SPL versus slant range for flight path B 0.5 sec before overhead position. Source directivity angle,  $71^\circ$ ; data symbols denote  $\frac{1}{2}$ -sec averaged data.

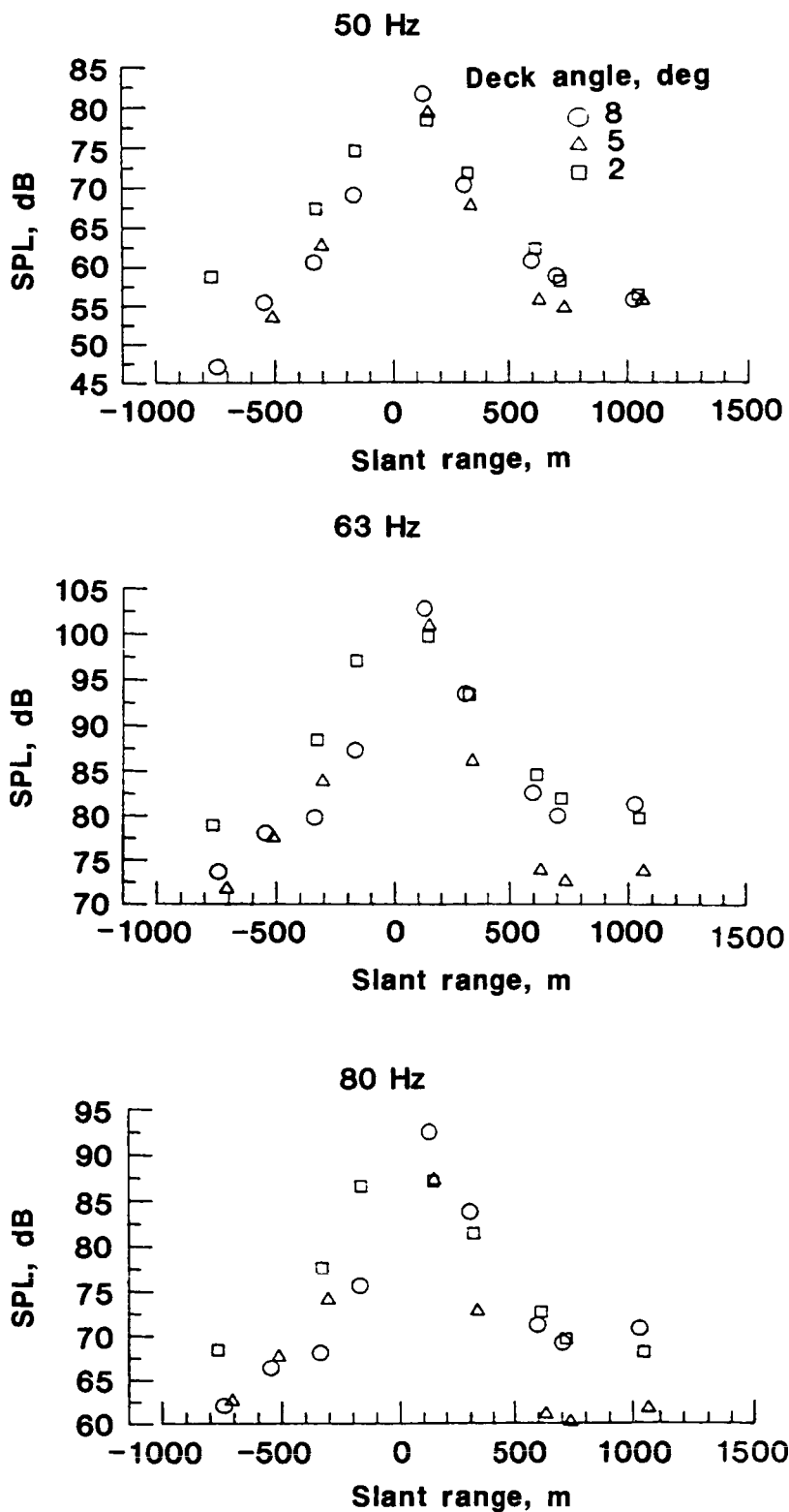


Figure A4. Results of one-third-octave-band SPL versus slant range for flight path B at overhead position (0 sec). Source directivity angle, 90°; data symbols denote 1/2-sec averaged data.

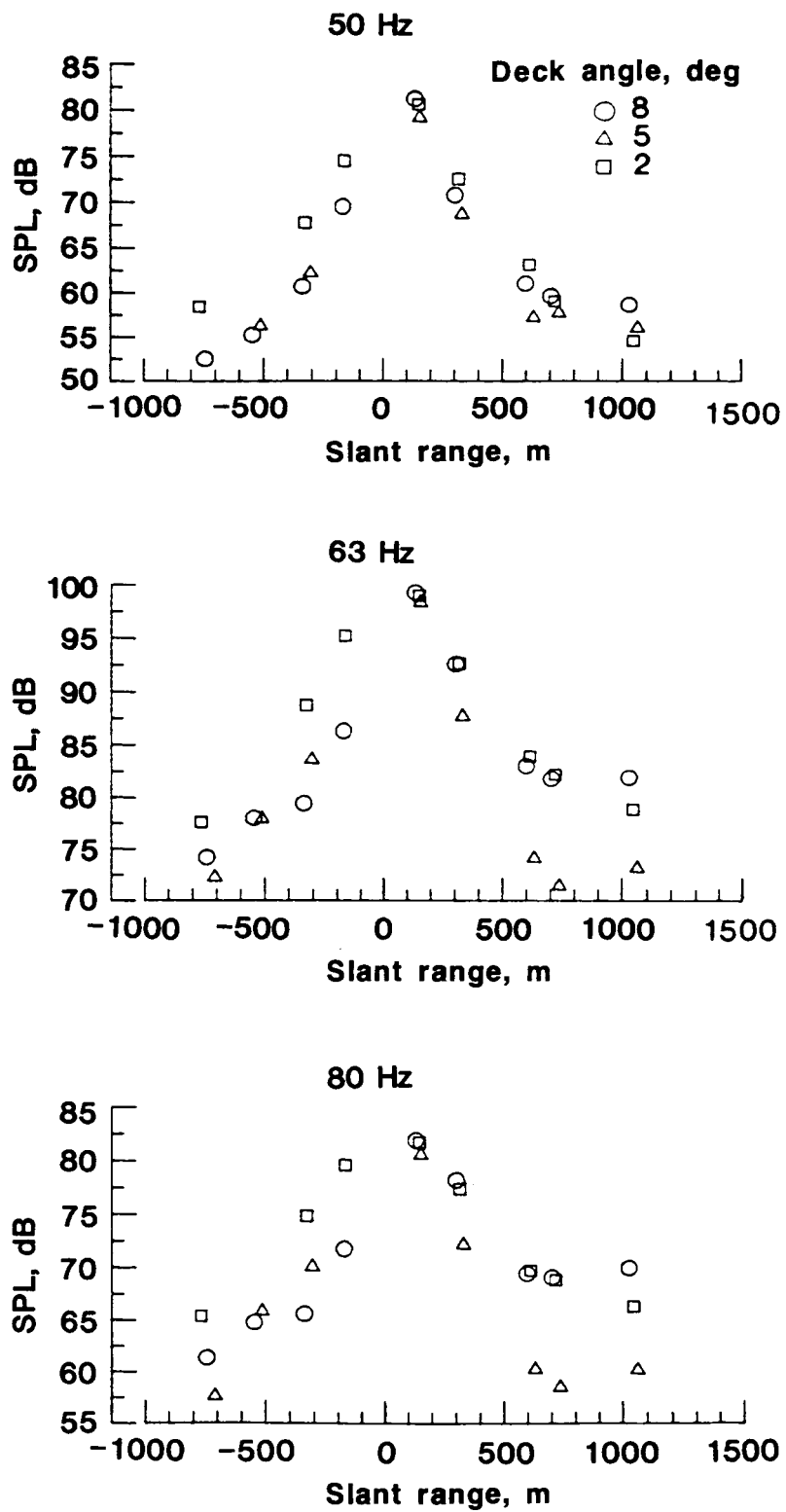


Figure A5. Results of one-third-octave-band SPL versus slant range for flight path B 0.5 sec after overhead position. Source directivity angle  $109^\circ$ ; data symbols denote  $\frac{1}{2}$ -sec averaged data.

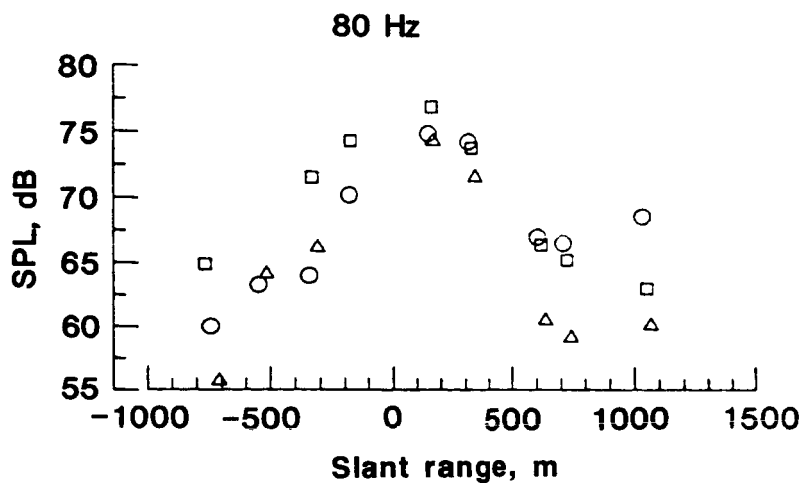
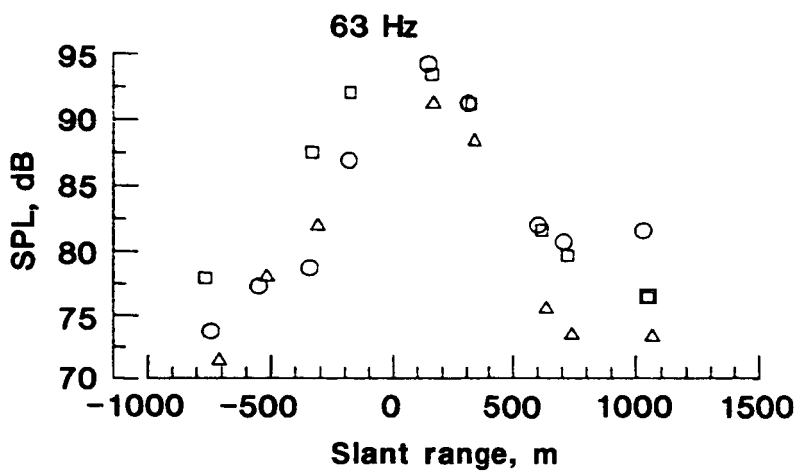
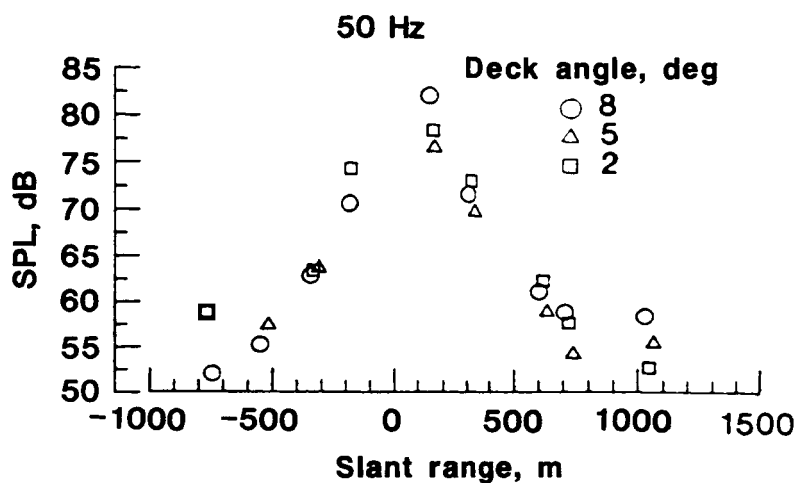


Figure A6. Results of one-third-octave-band SPL versus slant range for flight path B 1.0 sec after overhead position. Source directivity angle, 124°; data symbols denote 1/2-sec averaged data.

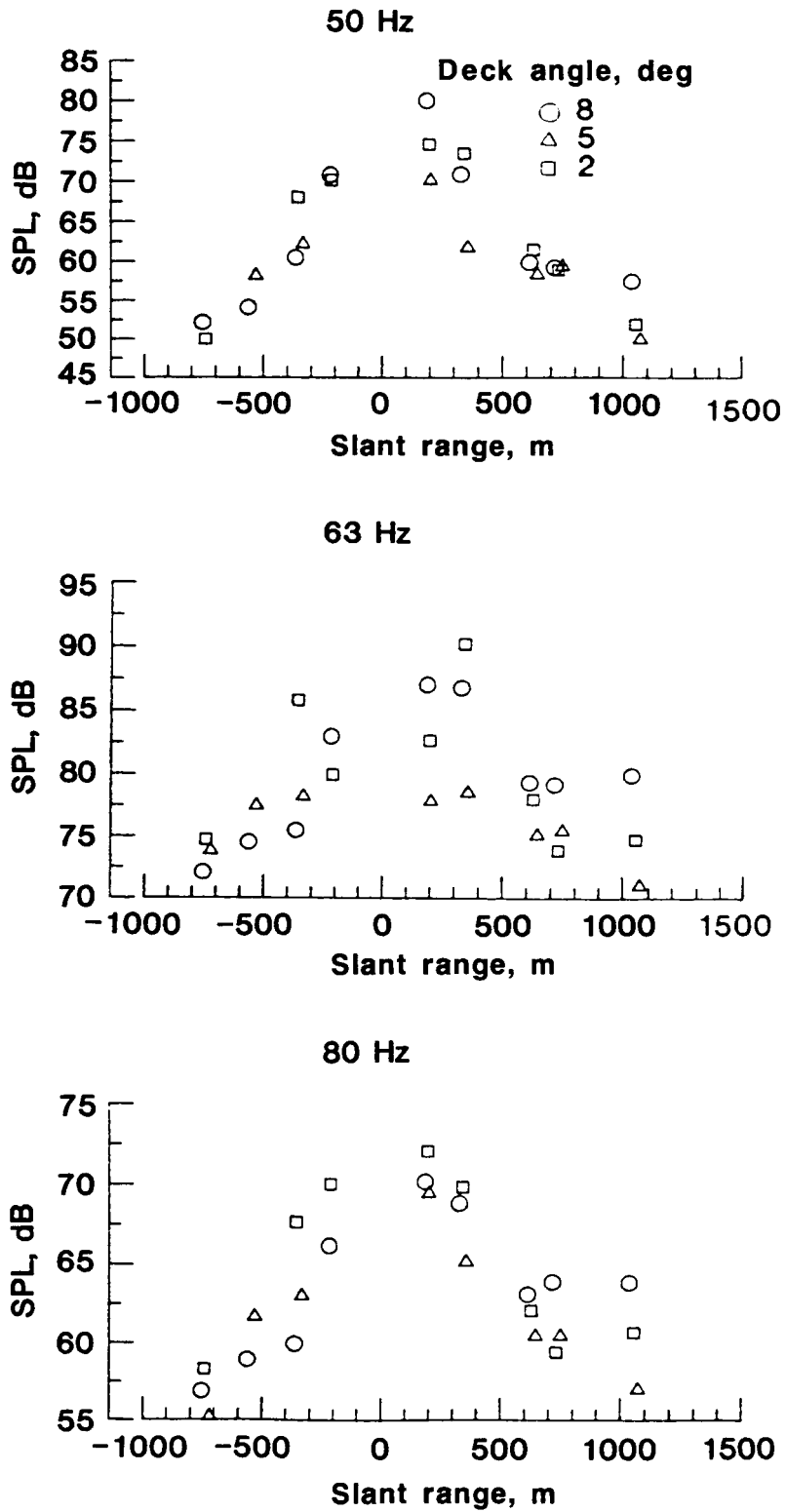


Figure A7. Results of one-third-octave-band SPL versus slant range for flight path B 2.0 sec after overhead position. Source directivity angle,  $144^\circ$ ; data symbols denote  $\frac{1}{2}$ -sec averaged data.

Standard Bibliographic Page

1. Report No. NASA TM-89035	2. Government Accession No.	3. Recipient's Catalog No.	
4. Title and Subtitle Noise Propagation From a Four-Engine, Propeller-Driven Airplane		5. Report Date February 1987	
		6. Performing Organization Code 505-63-91-02	
7. Author(s) William L. Willshire, Jr.		8. Performing Organization Report No. L-16179	
		10. Work Unit No.	
9. Performing Organization Name and Address NASA Langley Research Center Hampton, VA 23665-5225		11. Contract or Grant No.	
		13. Type of Report and Period Covered Technical Memorandum	
12. Sponsoring Agency Name and Address National Aeronautics and Space Administration Washington, DC 20546-0001		14. Sponsoring Agency Code	
		15. Supplementary Notes	
16. Abstract A flight experiment was conducted to investigate the propagation of periodic low-frequency noise from a propeller-driven airplane. The test airplane was a large four-engine, propeller-driven airplane flown at altitudes from 15 to 500 m over the end of an 1800-m-long, 22-element microphone array. The acoustic data were reduced by a one-third-octave-band analysis. The primary propagation quantities computed were lateral attenuation and ground effects, both of which become significant at shallow elevation angles. Scatter in the measured results largely obscured the physics of the low-frequency noise propagation. Variability of the noise source, up to 9.5 dB over a 2-sec interval, was the major contributor to the data scatter. The microphones mounted at ground level produced more consistent results with less scatter than those mounted 1.2 m above ground. The ground noise levels were found to be greater on the port side than on the starboard side.			
17. Key Words (Suggested by Authors(s)) Acoustics Propagation Ground effects Lateral attenuation Elevation angle Flight test		18. Distribution Statement Unclassified—Unlimited  Subject Category 71	
19. Security Classif.(of this report) Unclassified	20. Security Classif.(of this page) Unclassified	21. No. of Pages 42	22. Price A03